

Metal–Organic Framework Materials as Chemical Sensors

Lauren E. Kreno,[†] Kirsty Leong,[‡] Omar K. Farha,[†] Mark Allendorf,^{*,‡} Richard P. Van Duyne,[†] and Joseph T. Hupp^{*,†}

[†]Department of Chemistry, Northwestern University, 2145 Sheridan Road, Evanston, Illinois 60208, United States

[‡]Sandia National Laboratories, Mail Stop 9291, Livermore, California 94551-0969, United States

CONTENTS

1. Introduction	1105
1.1. Selecting MOFs for Sensor Applications	1106
1.2. Signal Transduction	1107
1.3. Fabrication of MOF Films	1107
2. MOF Sensors	1108
2.1. Solvatochromism/Vapochromism	1108
2.2. Luminescence-Based Sensing	1109
2.2.1. Photoluminescence	1109
2.2.2. Radioluminescence	1111
2.2.3. Interferometry	1113
2.4. Localized Surface Plasmon Resonance	1115
2.5. Colloidal Crystals	1116
2.6. Impedance Spectroscopy	1116
2.7. Electromechanical Sensors	1118
2.7.1. Quartz Crystal Microbalance	1118
2.7.2. Surface Acoustic Wave Devices	1119
2.7.3. Microcantilevers	1120
3. Conclusions and Future Outlook	1121
Author Information	1122
Biographies	1122
Acknowledgment	1124
References	1124

1. INTRODUCTION

Among the classes of highly porous materials, metal–organic frameworks (MOFs) are unparalleled in their degree of tunability and structural diversity as well as their range of chemical and physical properties. MOFs are extended crystalline structures wherein metal cations or clusters of cations (“nodes”) are connected by multtopic organic “strut” or “linker” ions or molecules. The variety of metal ions, organic linkers, and structural motifs affords an essentially infinite number of possible combinations.¹ Furthermore, the possibility for postsynthetic modification adds an additional dimension to the synthetic variability.² Coupled with the growing library of experimentally determined structures, the potential to computationally predict, with good accuracy, affinities of guests for host frameworks points to the prospect of routinely predesigning frameworks to deliver desired properties.^{3,4} MOFs are often compared to zeolites for their large internal surface areas, extensive porosity, and high degree of crystallinity. Correspondingly, MOFs and zeolites have been utilized for many of the same applications

including gas storage^{5,6} and separation⁷ as well as heterogeneous catalysis.⁸ Recently, several investigators have also begun exploring the potential of MOFs as chemical sensors. Although yet to be systematically exploited, the exceptional tunability of MOF structures and properties should constitute an important advantage over other candidate classes of chemo-sensory materials.

There are needs for sensitive and selective detection of gas and vapor phase analytes for a range of applications including industrial process management, chemical threat detection, medical diagnostics, food quality control, occupational safety, and environmental monitoring. The majority of commercialized sensors rely upon organic-polymeric or inorganic-semiconductor films that absorb or react with analyte molecules. Typically, changes in electrical, photophysical, or mechanical properties of these films are monitored. The magnitudes of the changes typically depend strongly on analyte concentration, as well as analyte chemical and physical characteristics such as acidity or basicity, propensity for donating or accepting electrons, and ability to permeate and swell films. While a variety of chemical sensors have been successfully commercialized, needs exist for improvement. For example, H₂ sensors based on reversible, dissociative uptake of H₂ by films of elemental palladium (and concomitant modulation of film resistivity, reflectivity, etc.) are susceptible to poisoning by CO and H₂S. Ubiquitous chemiresistive sensors, based on metal oxides, typically must be operated at high temperature (>200 °C) to promote reaction of surface-bound oxygen species.⁹ In addition, they typically exhibit cross-sensitivity and significant baseline drift over the life of the sensor. In principle, at least, MOFs can overcome many of the challenges of selectivity that plague other sensor materials. Many MOFs have also proven to be thermally robust, typically resisting decomposition at temperatures up to 300 °C or higher (and in a few cases to above 500 °C).^{10,11}

Herein, we present a critical review of the literature on MOFs as chemical sensors. We begin by briefly examining challenges relating to MOF sensor development including the design of MOFs with desirable properties, incorporation of appropriate signal transduction capabilities, and integration of MOFs into devices by employing thin-film growth techniques. Subsequent sections discuss specific examples of MOF sensors, categorized by method of signal transduction. Sensors based on MOF photoluminescence^{12–14} are discussed briefly. Because the linkers in most MOFs contain aromatic subunits that can readily luminesce following UV or visible (typically blue) excitation, it is

Special Issue: 2012 Metal-Organic Frameworks

Received: August 18, 2011

Published: November 09, 2011

not surprising that a very large number of MOFs have been found to be photoluminescent. Additionally, because photoexcitation of a typical linker entails transiently populating the linker's LUMO with a strongly reducing electron and forming a strongly oxidizing hole in the linker's HOMO, it is not surprising that intensities of photoluminescence from many MOFs can be greatly attenuated when the materials sorb molecules that are either easily oxidized or easily reduced. A primary limitation of these types of sensors is that they (usually) lack sufficient chemical selectivity. Another limitation is that they (usually) entail a loss of signal (i.e., fluorescence or phosphorescence intensity) in response to sorption of analyte molecules. A drawback of "turn-off" sensors is that phenomena other than analyte capture can result in loss of signals. With these issues in mind, we have limited our review of luminescence-based sensors to a small number of recent reports where the porous MOF architecture, or its chemical composition, imparts selective sensing capabilities. Scintillating MOFs that luminesce in the presence of radioactive analytes are also discussed. Other signal transduction schemes that utilize photons include various kinds of optical interferometry, analyte modulation of localized surface plasmon resonance energies, and solvatochromism. Mechanical signal-transduction schemes employed with MOFs include ones based on surface acoustic wave, quartz crystal microbalance, and microcantilever devices. Electrical schemes thus far have been limited to ones based on impedance spectroscopy.

1.1. Selecting MOFs for Sensor Applications

Important elements to consider in optimizing the performance and utility of chemical sensors are sensitivity, selectivity, response time, materials stability, and reusability. Highly porous materials such as MOFs should be inherently sensitive for gas or vapor detection because they effectively concentrate analyte molecules at higher levels than are present in the external atmosphere. In fact, several state-of-the-art field-portable analytical instruments used by military organizations to detect chemical threats incorporate a sample preparation step where the analyte is concentrated using a porous sorbent material.^{15,16} Direct detection of the analyte within the sorbent would simplify these portable systems. While sensitivity depends in part on the method of signal transduction, it also depends on the strength of analyte binding to the MOF (stronger binding translates into lower detection limits) and on the dynamics of analyte transport within the MOF. Exceptionally sluggish transport can lead to long response times that are difficult to distinguish from baseline drift. The maximum observable signal should depend in part on the sorption capacity of the MOF.

The potential selectivity of MOF materials for specific analytes, or classes of analytes, is substantial, but, as yet, is not highly developed. Among possible mechanisms of molecular (analyte) selectivity, the most intuitive is size exclusion (molecular sieving) wherein atoms or molecules that are smaller than the MOF's apertures can be adsorbed, but larger molecules cannot.¹⁷ Pore and aperture sizes are determined by MOF topology, node and linker sizes and shapes, linker appendages and their directional orientation, and framework catenation (i.e., interpenetration or interweaving of identical frameworks). In early work by Eddaoudi and co-workers, the IRMOF series was synthesized utilizing the same Zn₄O corner with struts of varying size and chemical functionality.¹⁸ The result was a progression of isostructural MOFs with aperture sizes ranging from 3.8 to 19 Å.

One important consideration for designing pore and aperture size is the tendency for MOFs with lengthier struts (which should produce larger apertures) to catenate, thereby yielding smaller pores. That catenation is common should not be too surprising, as MOFs should be nearly ideal templates for formation of replicas of themselves. Several strategies for suppressing framework catenation have been described, including: (a) the design of sterically hindered struts,^{19,20} (b) templating,^{21,22} (c) MOF assembly under conditions of high dilution,²³ and (d) inclusion of bulky linker appendages that can be thermally or photochemically cleaved after MOF assembly.^{24,25} Pore dimensions can also be modulated by removing nonstructural ligands (e.g., coordinated solvent molecules) from framework nodes or replacing node-coordinated solvent molecules with larger or smaller ligands.²⁶ It is worth noting that, all else being equal, small pores will adsorb gas or vapor analytes more strongly than will large ones, and thereby enhance sensitivity.

Another source of selectivity is chemically specific interactions of the adsorbate with the MOF internal surface, for example, via hydrogen bonding, Mulliken-type electron donor/acceptor interactions, or formation of coordinate-covalent bonds. Often, the desired functionality can be incorporated at the MOF-synthesis stage. For example, Zn(bptc) (bptc = 4,4'-bipyridine-2,6,2',6'-tetracarboxylate) was shown to preferentially adsorb polar molecules and those with conjugated π systems.²⁷ These interactions were attributed to H-bond and π–π interactions, respectively, between the guests and MOF struts. However, some functional groups cannot be readily incorporated during materials synthesis due to their tendency to coordinate to the MOF corners and form undesired structures. To overcome this problem, several methods entailing postsynthetic modification of MOFs have been developed. Some involve alteration or addition of functional groups on struts;^{28,29} others are node-based and entail binding pore-modifying molecules at coordinatively unsaturated metal sites at the MOF.^{26,30}

Last, certain potential analytes may be preferentially adsorbed if they favorably interact with open metal sites in the MOF. These can involve reversible bonding interactions, for example, NO binding to Co(II), Cu(II), or Ni(II).³¹ Or, they can be based on purely electrostatic interactions, such as quadrupole/charge interactions between CO₂ molecules and cobalt or aluminum ions.^{32,33} When designing MOFs for selective sensing applications, the existing literature on gas separation by MOFs⁷ can offer insight into what structures and functionalities may be useful.

The final requirements of rapid response time and sensor regeneration are dependent on sorption kinetics and thermodynamics. Because most guests are physisorbed, MOF sensors should be recyclable simply by subjecting the material to dynamic vacuum, if necessary, at slightly elevated temperature. The response rate is governed by the rate of guest diffusion within the pores and by MOF particle size or film thickness. (Recall that diffusion times increase as the square of diffusion distance.) Although we have cited only a few, several studies of molecule diffusion within MOFs have been reported, based on either theoretical modeling^{34–36} or experimental measurements.^{37,38} Lin and co-workers have shown that diffusion times can be shortened by increasing MOF aperture sizes.³⁹ Lee and co-workers have reported on materials within which diffusion is highly anisotropic, differing in the *x*, *y*, and *z* directions.⁴⁰ While their report focuses on implications for kinetic separation of hydrocarbons, it is obvious that there can be implications for sensing as well.

By way of example, diffusivities of small alkanes in HKUST-1 ($\text{Cu}_3(\text{btc})_2(\text{H}_2\text{O})_3$, btc = benzenetricarboxylate; also known as Cu-BTC) fall in the range of $\sim 10^{-9} - 10^{-8} \text{ m}^2 \text{ s}^{-1}$ ³⁵ with the diffusivity of methanol in a manganese formate MOF measured at $1.5 \times 10^{-12} \text{ m}^2 \text{ s}^{-1}$ ⁴¹ and pyridine in HKUST-1 reported even smaller at $1.5 \times 10^{-19} \text{ m}^2 \text{ s}^{-1}$.³⁸ Returning to hydrocarbons, Snurr and co-workers have shown that diffusion coefficients for linear alkanes within MOFs systematically decrease with increasing chain length.³⁵ It is also important to recognize that values for diffusion coefficients are somewhat loading-dependent, with smaller values typically found at higher loadings. Slower diffusion rates are also expected when MOF materials are infiltrated with solvent molecules (that must be displaced for analyte molecules to enter and diffuse within the material). Diffusion-based mass-transport resistance effects could have significant negative consequences for sensor response time. Bearing this in mind, both thin film and bulk crystalline MOF sensors should be designed with small enough dimensions to ensure rapid analyte uptake and equilibration.

Not unlike other nanoporous materials, MOFs have the ability to adsorb large quantities of water; for example, it is reported that HKUST-1 can adsorb as much as 40 wt % water.^{42,43} As will be seen below, this makes them attractive for humidity sensing, which has been demonstrated using a variety of sensing platforms.^{44,45} However, water vapor is also a common interfering gas and must be addressed in the design of MOF-based sensing systems. Although a legitimate concern, the synthetic flexibility of MOFs suggests a number of possible solutions to this problem (in addition to simply removing water vapor prior to the sensor). For example, hydrophobic MOFs, such as the ZIF materials,⁴⁶ could be used. Alternatively, “fingerprint” approaches could be employed, in which the response of an array of sensors coated with different MOFs is used to positively identify a molecule in the presence of other species. For example, recent computational modeling suggests that two different MOFs can be used to selectively detect compounds of similar chemical structure, such as TNT and xylenes.⁴⁷ A third approach could take advantage of the properties of luminescent MOFs by causing molecule-specific shifts in the luminescence spectrum or formation of new photoemission.⁴⁸ Clearly, MOFs are at a very early stage in their development with respect to chemical sensing, and practical problems of this nature will have to be solved before MOFs can proceed from the realm of laboratory synthesis to practical implementation.

1.2. Signal Transduction

Despite the numerous properties of MOFs that suggest them as attractive chemo-sensory materials, their implementation has been largely limited by one major challenge: signal transduction. The majority of MOF sensors that have been reported are based on luminescence quenching of lanthanide ions or aromatic fluorophores used as corners and struts, respectively. In these cases, the MOF is serving two functions: receptor and transducer. That is, it both recognizes molecules and produces a signal. Many MOFs produce insignificant luminescence or else show substantial changes in luminescence in response to uptake of only a few kinds guests (e.g., good electron donors or acceptors), so this is not a generalizable approach. A few examples of MOFs that change color depending on the type of guest have also been reported;^{49–51} however, most MOFs do not exhibit such behavior. To utilize other MOF materials for chemical detection, some external means of signal transduction must be incorporated.

Several kinds of transduction schemes can be envisioned, including optical, electrical, and mechanical schemes. Optical transduction modes that have been applied to MOFs include sensors based on interferometry⁴⁶ and localized surface plasmon resonance (LSPR) spectroscopy.⁵² The first reported example of the former relied upon fabrication of the MOF as a thin film such that reflections off of the front and back surfaces of the film produced wavelength-dependent interferences.⁴⁶ In the case of an LSPR sensor, the MOF was attached to a plasmonic nanoparticle surface, and the wavelength-dependent extinction of the nanoparticle was used to detect changes within the MOF.

Although electrical and electrochemical methods have been widely used in sensors based on solid electrolytes, chemiresistive metal oxides, and metal–oxide–semiconductor field-effect transistors, they have been minimally explored for MOFs. This is most likely because the majority of MOFs are insulating. However, development of conductive MOFs (typically ion conducting) is currently underway for other applications such as proton exchange membrane fuel cells.⁵³ To our knowledge, only one group has reported measurement of MOF electrical properties as a means of chemical sensing.⁵⁴ In that case, only one of three screened MOFs exhibited solvent sensing behavior. Last, mechanical sensors are appealing for their amenability to miniaturization and multiplexing. MOFs have been grown on piezoresistive microcantilevers⁴⁴ and quartz crystal microbalances,^{38,55,56} which convert changes in crystal size or mass into an electrical signal.

In principle, any MOF property that changes depending on the guest could be measured as a sensing signal. For example, MOFs with guest-dependent magnetism, including structures that exhibit spin crossover, have been suggested as chemical sensors.^{57,58} However, this Review focuses mainly on reports where sensing was the specific intent.

1.3. Fabrication of MOF Films

Many signal transduction schemes require a physical interface between the MOF and a device. This generally involves fabricating the MOF as a thin film on a surface. The increasing interest in utilizing MOFs as sensors or as selective membranes has led to a surge of interest in preparing MOF thin films.^{59,60} Most commonly, MOF films have been synthesized directly on the surface of interest from the appropriate molecular and ionic precursors. Typically the surface is a metal, metal–oxide, glass, or silicon. Film formation can sometimes be accomplished by simply placing a platform in a reactor with the MOF precursors. These direct growth approaches often require functionalization of the surface with a self-assembled monolayer or seeding of the growth with small MOF crystals to nucleate film formation. In some cases, MOF films can be grown one molecular or ionic layer at a time by sequential immersions in solutions of the metal and organic precursors.⁶¹ Functional groups on the surface (e.g., terminal components of self-assembled monolayers) may nucleate MOF growth in a specific crystallographic direction, leading to preferentially oriented films.^{62–64} Surfaces also can occasionally template for MOF architectures that are different from those obtained from conventional syntheses.⁶⁵ Fischer and co-workers showed, for example, that the form of $\text{Zn}(\text{bdc})(\text{bpy})_{0.5}$ (bdc = benzenedicarboxylate, bpy = 4,4'-bipyridine) grown on a surface is a single framework material, in contrast to the bulk MOF, which shows 2-fold interpenetration.²² As a result, the surface-bound MOF has larger pores and nearly twice the internal surface area. These nuances could have

significant implications for MOF sorption behavior and sensor selectivity.

A second method for film fabrication is to first synthesize small MOF particles and subsequently deposit them on a surface. This has been demonstrated, for example, for Cr-MIL-101 where a suspension of monodisperse nanoparticles was obtained by microwave heating and then layered onto Si wafers via repetitive dip-coating.⁶⁶ Similar techniques have been used for ZIF-8 film formation,⁴⁶ where particle growth may nucleate on the surface while also incorporating particles formed initially homogeneously in solution; however, the exact mechanism is unknown. Our own experience with these methods has been that they are remarkably reproducible with regard to both average film thickness and uniformity of film thickness.

An unusual, but useful, third approach involves MOF film formation within the spatial constraints of a gel layer.⁶²

2. MOF SENSORS

2.1. Solvatochromism/Vapochromism

One of the simplest, and arguably most powerful, means of transducing a sensing signal is a visible change in a material's color. Solvatochromism refers to a large shift in the absorption spectrum of a material in response to a change in the identity of the solvent. Often the shifts correlate with empirical measures of solvent polarity, implying that the electronic transition responsible for the coloration entails charge transfer, that is, a change in dipole moment upon excitation from the ground to the excited electronic state of the chromophoric component of the material. If the excited state features a larger dipole moment than the ground state, it is preferentially stabilized by polar solvents, and bathochromic shifts (red shifts) are observed with increasing solvent polarity. Conversely, if the ground state has the larger dipole moment, hypsochromic shifts (blue shifts) occur with increasing solvent polarity. For a chromophore embedded in a MOF (for example, as a linker), sorption of vapor is the equivalent of solvating a molecular absorber, and vapochromic trends should match solvatochromic ones.

As an example, Lu et al. synthesized a copper MOF containing the ligand 3,6-di(pyridin-4-yl)-1,2,4,5-tetrazine (dptz), which shows solvatochromic behavior when immersed in solvents ranging in polarity from water to chloroform (shown in Figure 1).⁴⁹ Overall, the material shows a negative solvatochromic effect with the absorption band blue-shifting with increasing solvent polarity. Two distinct groupings were observed, one for hydroxyl and one for nonhydroxyl solvents, when the measured band gaps were plotted versus solvent polarity.

In addition to traditional solvatochromic effects based on solvent polarity and specific solvent–chromophore interactions, MOFs have displayed solvent-dependent color changes stemming from other mechanisms. Because MOFs contain metal ions in addition to their organic components, they have characteristics similar to discrete coordination complexes, and changes in the coordination sphere of these metal centers can play a role in MOF sensing. Early in the MOF literature, Long and co-workers showed that exposing Co^{2+} MOFs to various vapors could shift the optical absorption across the visible region.⁵⁰ The explanation was a change in coordination environment from the as-synthesized octahedral to a tetrahedral geometry.

A similar mechanism of color change is proposed in a recent paper by Lee et al. reporting on a MOF that senses chloride ions derived from chlorine-containing vapors or gases. The MOF

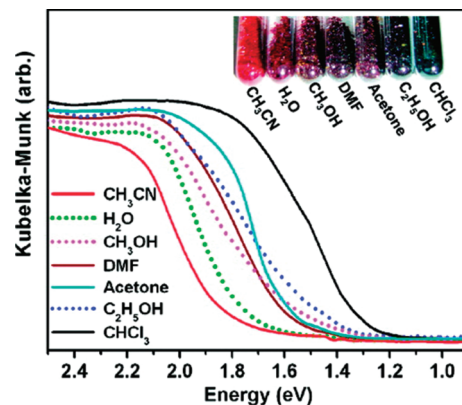


Figure 1. Visible spectra and photograph of MOF crystals containing solvents (condensed vapors). A negative vapochromic effect is observed for both hydroxyl and nonhydroxyl vapors (solvents). Reprinted with permission from ref 49. Copyright 2011 American Chemical Society.

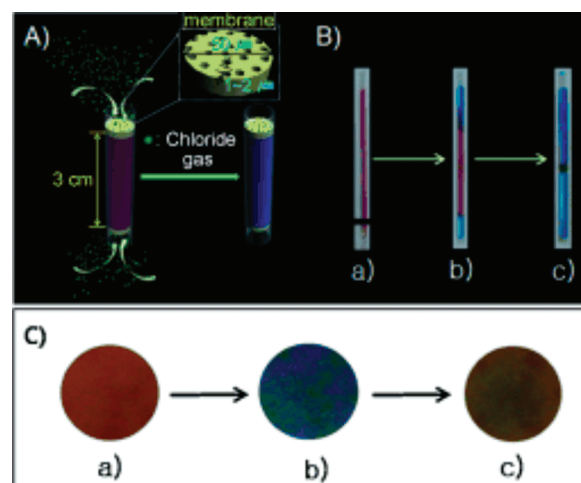


Figure 2. (A) Cartoon of MOF-coated capillary for sensing chloride gas. (B) Photo of capillary as made (a), after 10 s (b), and after 30 s (c) exposure to 100 mM chloride-containing vapor or gas. (C) Photo of MOF pellet as made (a), after exposure to phosgene gas (b), and after rinsing with 100 mM HBr to regenerate original structure (c). Reprinted with permission from ref 51. Copyright 2011 Wiley-VCH.

contains Co^{2+} nodes coordinated to 1,2,4,5-tetra(2H-tetrazole-5-yl)-benzene (TTB) struts as well as Br^- anions.⁵¹ It is obtained as an amorphous gel (via standard sol–gel chemistry), rather than as crystalline compound, and so, strictly speaking, may not fit the definition of a MOF. As synthesized, the material is characterized by a visible absorption peak at 475 nm, suggesting octahedral coordination of the Co^{2+} centers. Interestingly, when the coordination polymer is exposed to chlorine-containing gases, including HCl , SOCl_2 , $(\text{COCl})_2$, and COCl_2 (phosgene), its color changes from red to blue (see Figure 2). A new absorption feature appears at 670 nm, creating the blue color. The authors attribute this absorption peak to tetrahedrally coordinated Co^{2+} . To explain the change in metal coordination geometry, they hypothesize that the Br^- is replaced with Cl^- originating from the reactive gases.

Several aspects make this chemosensory material promising. First, the color change is rapid and easily visible by eye.

The calculated limit of detection for phosgene is as low as 1 ppb. In addition, the sensor can be regenerated by washing with HBr to reform the original compound, as shown in Figure 2. Perhaps most intriguing is the hypothesis that chloride from these harmful gases is being incorporated into the MOF structure, implying that the hazardous analyte is being destroyed (albeit, likely only stoichiometrically rather than catalytically).

2.2. Luminescence-Based Sensing

2.2.1. Photoluminescence. Virtues of MOFs as Active Materials in Luminescence-Based Chemical Sensors. Luminescent frameworks are by far the most widely explored type of MOF sensor to date. The popularity of luminescence over other transduction mechanisms is a consequence of several key elements, such as the production of a signal that is visible by eye. Fluorescence spectroscopy is well established, and detection limits can reach the single molecule level. Another virtue is the ability to address powdered materials directly, that is, without the need for film fabrication or other processing. Thus, conventional solvothermal syntheses can be employed to create luminescent MOFs. In principle, the porous crystalline MOF architecture provides advantages over other sensor materials. The tunability of MOF sorption properties offers (in principle) a high degree of molecular specificity. Toward that goal, two groups of researchers have shown how molecular sieving can be used for size-selective sensing in luminescent Zn_3btc_2 ($btc =$ benzenetricarboxylate).^{67,68} Following exposure to amines of different sizes, a decrease in the fluorescence was observed for amines that were small enough to easily diffuse into the MOF pores, including ethylamine, dimethylamine, and propylamine. In contrast, aniline and butylamine showed no quenching, presumably due to size exclusion.

A similar size-selective effect has been observed for a Cd^{2+} -based MOF.⁶⁹ Introduction of various anions revealed that only nitrite quenches the luminescence. While the investigators speculated energy transfer (to NO^{2-}) through strut-based C–H bonds that purportedly engage in hydrogen bonding with nitrite ions, a more plausible mechanism, in our view, is reductive quenching of the highly energetic excited state by nitrite.

In addition to size-selectivity of MOFs, their large surface areas combined with confinement of the analyte inside the MOF cavities can potentially translate to high sensitivity. Last, the extended three-dimensional structure may well facilitate dipolar coupling between neighboring linkers, thereby enabling strut-to-strut energy transfer (Förster transfer) on a time scale that is short as compared to the singlet excited-state lifetime. Thus, one analyte binding event could affect several signaling centers, analogous to what has been demonstrated for conjugated fluorescent polymers.⁷⁰

Mechanisms of Luminescence Sensing in MOFs. Rational design of these architectures draws from the myriad examples of discrete luminescent coordination complexes. In both the molecular and the MOF cases, there can be multiple sources of luminescence. Linker-based fluorescence is common due to the fact that many MOFs contain conjugated ligands that absorb in the visible or UV, together with d^{10} metal ions such as $Zn(II)$ or $Cd(II)$ (i.e., largely electronically inert ions). Metal-centered luminescence (mainly phosphorescence) is seen primarily in MOFs containing f-elements as nodes. In many cases, highly absorbing (i.e., conjugated) struts coordinated to these centers behave as antennas, amplifying emission via metal-facilitated (spin-orbit coupling facilitated) intersystem crossing from

singlet to triplet excited states of the struts, followed by ligand-to-metal energy transfer.

The most common form of signal transduction in luminescent MOFs is quenching, or occasionally enhancement, of photo-induced emission due to guest adsorption. The strength of these effects can depend on the nature of the host–guest interactions. Typically, the relevant interactions are ones that allow for significant electron-donor/electron-acceptor orbital overlap, where the MOF or analyte may play either role. As a consequence, the most readily detected analytes are those that are good electron donors (e.g., amines) or acceptors (e.g., nitroaromatics, including common explosives or simulants). Alternatively, a guest may serve to alter the redox potential of a built-in (i.e., pendant to strut) donor or acceptor, thereby inhibiting quenching and enhancing luminescence. In rare cases, adsorbates engender shifts in the frequency of the MOF emission. This type of signal transduction is inherently more attractive than luminescence quenching (“turn-off” sensing) because, by appropriate single-wavelength monitoring (i.e., at the peak of the shifted emission band), analyte uptake can be read out as an increase in the intensity of luminescence. Yet another luminescence-based mechanism for signal transduction involves the association of an adsorbate molecule with a framework strut to form an exciplex with a unique emission band.

Sensing by Luminescence Quenching/Enhancement. Numerous groups have reported sensing of vapor-, liquid-, and solution-phase analytes by fluorescence quenching or enhancement. Both lanthanide and transition metal MOFs have exploited these effects to sense organic solvents, aromatics, water, and ions. To our knowledge, O_2 is the only purely gas-phase analyte reported to be sensed by a luminescent MOF.^{71,72} Xie et al. incorporated phosphorescent complexes of iridium(III) into a MOF as struts and showed that emission is quenched by energy transfer to O_2 .⁷¹ The responsiveness of the porous material to dioxygen, and its absence of sensitivity to dinitrogen, is a consequence of the triplet electronic configuration of ground-state O_2 (versus singlet configurations for most other molecules). An and co-workers similarly reported the O_2 quenching of Yb^{3+} ions that had been postsynthetically encapsulated in the pores of a Zn -adenitate MOF.⁷²

Recently, Lan and co-workers reported two fluorescent Zn -based MOFs capable of sensing nitro-containing molecules relevant to detection of explosives.^{73,74} Detection of hazardous materials is a significant concern for homeland security, and portable sensors are potentially desirable to circumvent the complexity sometimes associated with traditional analytical methods. In the case of explosives, identification can be accomplished by detecting a byproduct or additive when the explosive itself is not readily detectable (e.g., due to low vapor pressure). $Zn_2(bpd)_2bpee$ ($bpd =$ 4,4'-biphenyldicarboxylate; $bpee =$ 1,2-bipyridylethene), a MOF containing a linker with the potential to fluoresce, was screened for the detection of 1,4-dinitrotoluene (DNT), which is a byproduct of the formation of 2,4,6-trinitrotoluene (TNT) and 2,3-dimethyl-2,3-dinitrobutane (DMNB). The latter is an additive used to facilitate detection of plastic explosives.⁷³ In its solvent-evacuated state, the MOF shows an emission band centered at 420 nm. Upon exposure to 0.18 ppm DNT or 2.7 ppm DMNB, the emission red shifts and decreases in intensity due to electron transfer from the struts to DNT and DMNB guests. The fluorescence quenching efficiency saturates at 85% for DNT and 84% for DMNB, within 10 s as shown in Figure 3. Quenching efficiency is defined as $(I_0 - I)/I_0 \times 100\%$,

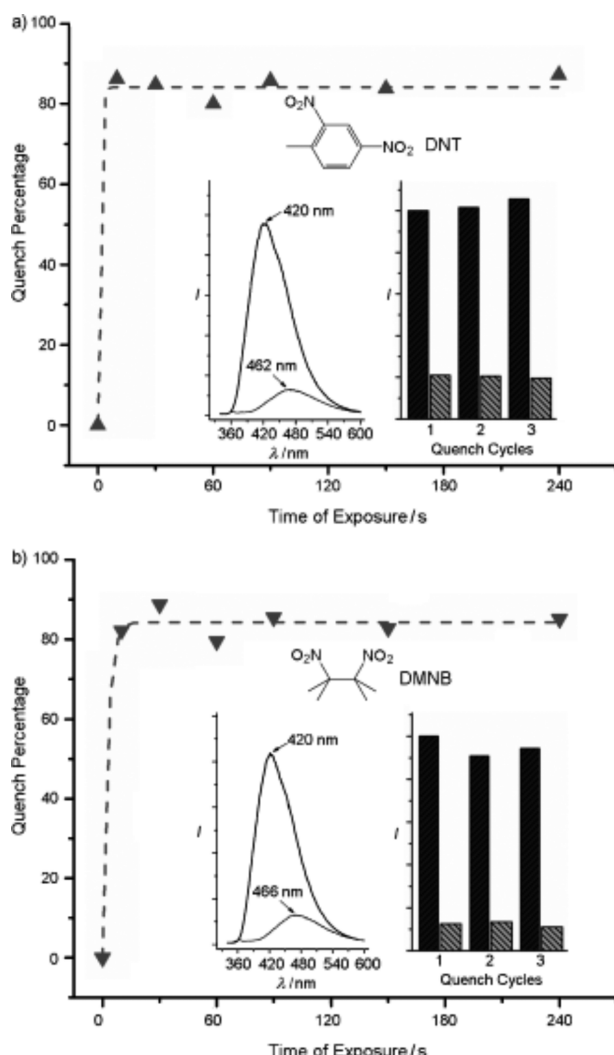


Figure 3. Time-dependent fluorescence quenching by (a) 2,4-dinitrotoluene (DNT) and (b) 2,3-dimethyl-2,3-dinitrobutane (DMNB) in a luminescent MOF. Insets: Fluorescence spectra before and after exposure to the analyte vapor for 10 s (left), and three consecutive quench/regeneration cycles (right). Reprinted with permission from ref 73. Copyright 2009 Wiley-VCH.

where I_0 is the intensity before exposure, and I is the intensity following exposure.

Remarkably, this sensor exhibits sensitivity comparable to conjugated polymer films for the detection of DNT and outperforms them in terms of response time. In addition, this sensor displays unparalleled sensitivity to DMNB, which is notoriously difficult to detect, possibly due to poor $\pi-\pi$ interactions and subsequently weak binding. Importantly, both analytes adsorb semireversibly; that is, the initial fluorescence is recoverable by heating at 150 °C.

More recently, the same group measured the quenching effect of various substituted aromatics on $[\text{Zn}_2(\text{oba})_2(\text{bpy})] \cdot \text{DMA}$ [$\text{H}_2\text{oba} = 4,4'$ -oxybis(benzoic acid); bpy = 4,4'-bipyridine; DMA = N,N' -dimethylacetamide].⁷⁴ This pillared paddle-wheel MOF emits at 420 nm. When exposed to a range of aromatic analytes, it was found that all nitro-containing molecules quench the fluorescence to varying degrees, as shown in graphical form in Figure 4. The quenching efficiency increased in the order

DNT < *p*-dinitrobenzene ≈ nitrotoluene < *m*-dinitrobenzene < nitrobenzene. This trend was rationalized on the basis of both the electron-withdrawing ability of the analyte and its vapor pressure. The dinitrobenzenes are highly electron deficient and therefore should be good oxidative quenchers, but they have low vapor pressures. Nitrobenzene has a higher quenching efficiency (despite having one fewer $-\text{NO}_2$ group) presumably because of its relatively high vapor pressure. The nitrotoluenes are less electron-deficient due to the electron-donating methyl substituents, so they quench less efficiently.

While the rationalizations are persuasive, the underlying assumption that greater vapor pressure for one analyte versus another will lead to greater uptake of the former is a potentially unreliable one. Briefly, the problem is that the extent of analyte uptake depends not only on the analyte vapor pressure, but also, of course, on the adsorbate/adsorbent binding constant. For related compounds, these constants often correlate inversely with vapor pressure (i.e., lower vapor pressure (at a given temperature) → higher binding constant). Expressed another way, molecules that adhere well to each other, for example, via London dispersion, will often also adhere well to adsorbents via the same kinds of interactions. One consequence is that detection limits (in terms of vapor-phase concentration) typically are lower for less volatile compounds. (Thus, vapor-phase detection limits for TNT typically are lower than for nitrobenzene if detection entails analyte sorption, for example, by a chemosensory polymer.)

In contrast to quenching behavior by analytes featuring electron-withdrawing substituents, those featuring electron-donating substituents (or at least lacking nitro substituents) were found to enhance the MOF fluorescence, with enhancement increasing in the order chlorobenzene < benzene < toluene (see Figure 4). Perhaps by analogy to the behavior of luminescent, wide-bandgap metal–oxide semiconductors (e.g., chemosensory behavior of zinc oxide), the authors attempted to interpret their findings in terms of analyte interactions with, and energetics relative to, the conduction band of the MOF; that is, the MOF is viewed as a semiconductor. For metal–oxide semiconductors, luminescence can be enhanced by adsorbates via pacification of surface states that otherwise function as electron/hole recombination centers. Alternatively, adsorbates can donate electron density, thereby engendering band bending. In turn, the band bending can drive charge separation, thereby slowing subsequent nonradiative recombination and allowing radiative recombination (luminescence) to play a greater role. While mechanisms this specific are not proposed in the original report, it is important to recognize that band bending can occur only if the semiconductor is doped. There is no obvious basis for doping to occur in the MOF, nor is there an obvious analogue to surface states.

Additionally, while calculations for the MOF may indicate band structure, the bands almost certainly are so narrow that the MOF is better represented as a collection of independent molecular chromophores (struts), with d^{10} metal ions ($\text{Zn}(\text{II})$) ions) behaving electronically as insulators. Luminescence spectroscopy of MOFs composed of stilbene dicarboxylate linkers connected to $\text{Zn}(\text{II})$ ions is consistent with this interpretation.⁷⁵ What is increasingly described in the MOF literature as an optical bandgap (i.e., valence-band/conduction-band separation energy) is probably better described as the HOMO/LUMO energy gap for single linkers acting as chromophores. Some of the incentive for ascribing meaningful band structure (and, by inference,

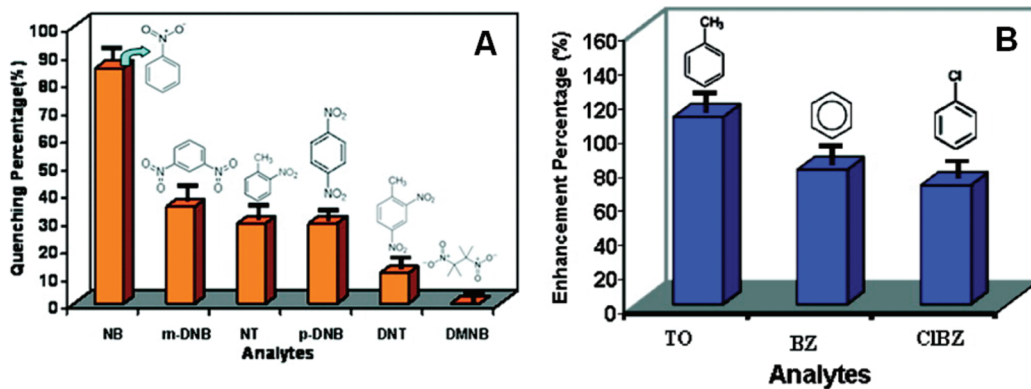


Figure 4. (A) Fluorescence quenching percentage by electron-deficient analytes, and (B) fluorescence enhancement percentage by electron-rich analytes in a luminescent MOF. Reprinted with permission from ref 74. Copyright 2011 American Chemical Society.

significant linker–linker electronic coupling and delocalization) likely comes from the shifts in the onset energy for electronic absorption when molecular linkers are incorporated in MOFs. A more prosaic interpretation would be to ascribe the spectral shifts to electrostatic perturbations of localized HOMO and/or LUMO energies by the highly charged metal ions constituting the MOFs' nodes.

Assuming that a semiconductor description is not suitable, we suggest the following: Fluorescence attenuation is caused by redox quenching of the single-linker-localized excited state by analytes that are good electron donors, that is, analytes that are comparatively easy to oxidize. The observed fluorescence enhancements upon adsorption of guests like toluene cannot be due to electron transfer in the opposite direction (i.e., from photoexcited linker to proximal analyte molecule) as this behavior would instead cause the MOF fluorescence to be attenuated. A more plausible interpretation is that sorbed molecules inhibit linker motions (vibrations, torsional displacements, etc.) that otherwise facilitate nonradiative decay of the photoexcited state. Behavior of this kind is often observed when molecular fluorophores are immobilized in (and rigidified by) polymeric films or glassy solvents. If sorbed analyte molecules exert a similar rigidifying effect, then nonradiative decay processes should be slowed and the fraction of excited species decaying radiatively should increase, resulting in increased fluorescence intensity.

Sensing by Exciplex Formation. Because most luminescent MOF sensors rely simply on the efficiency of fluorescence quenching, it can be difficult to distinguish between similar analytes that generate the same effect. To overcome this problem, Takashima et al. developed a luminescent MOF for which the emission frequency depends on the chemical identity of the guest molecule.⁷⁶

The chemosensory material examined was a 2-fold interpenetrated version of $Zn_2(bdc)_2(dpNDI)$ ($bdc = 1,4\text{-benzenedicarboxylate}$; $dpNDI = N,N'\text{-di(4-pyridyl)-1,4,5,8-naphthalenediimide}$). NDI is known to generate exciplex emission when interacting with aromatic molecules in solution, and these characteristics are transferred to the MOF structure. The MOF was soaked in a range of pure aromatic compounds containing different substituents. The analytes include benzonitrile, toluene, benzene, anisole, iodobenzene, and xylenes. In all cases except for benzonitrile, a new broad absorption peak between 420 and 500 nm was observed, indicating a ground-state charge transfer (CT) interaction between NDI and the guest. Each analyte also

exhibited exciplex emission, but at different wavelengths. As shown in Figure 5, the exciplex emission systematically shifted to longer wavelength with increasing electron-donating capability of the analyte (as measured, for example, by the analyte's ionization energy). The one exception to this correlation is iodobenzene. The heavy atom effect, in the form of singlet/triplet excited-state mixing facilitated by spin–orbit coupling, facilitates intersystem crossing and results in radiative decay via phosphorescence rather than higher-energy fluorescence.

What makes this material particularly interesting is that it displays superior properties as compared to the free NDI ligand, which can also be used to detect these analytes. Confinement of the guests within the MOF pores causes an enhancement of all of the fluorescence intensities, perhaps by rigidifying the exciplex and limiting vibrational motion associated with nonradiative decay of the photoexcited state. Conveniently, NDI itself (and consequently, the MOF in this case) has a fairly low fluorescence quantum yield. As a result, the as-synthesized MOF is in its dark state, with the fluorescence signal turned on by guest adsorption. Because each guest produces a different color of emission, it should be straightforward to establish the analyte's identity and its concentration by measuring the emission frequency and intensity.

2.2. Radioluminescence. MOFs present an opportunity to make significant advances in the detection and identification of subatomic particles for applications in nonproliferation, space exploration, nuclear power, and biology. The synthetic flexibility of MOFs allows them to be tailored in ways that are not possible in conventional scintillator materials, which include organic liquids, plastics, and inorganic materials such as sodium iodide. In addition, their crystalline structure allows the interactions among luminescent linkers to be characterized with subangstrom precision, creating a “nanolaboratory” for probing photophysics at a level of detail unimaginable with noncrystalline materials. As a result of these new degrees of freedom, which encompass both micro and meso length scales as well as the nanopore volume, rational design of both light output and timing in MOFs is achievable.

Scintillation is defined as the emission of short (ns) bursts of light in response to ionizing radiation (energy typically >10 eV) and in MOFs originates in the organic linkers. A few examples of luminescent linker groups that are similar to well-known organic scintillators are shown in Figure 6 (there are many more possibilities; see ref 12), from which it is evident that the

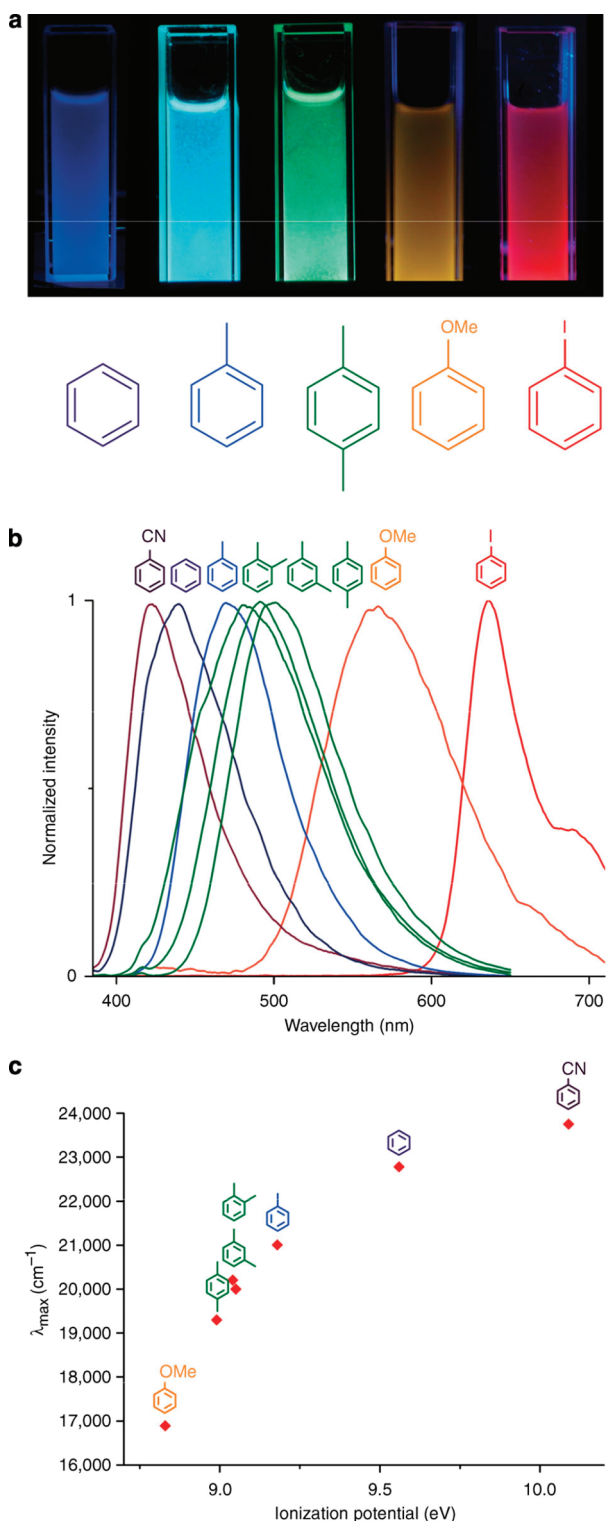


Figure 5. (a) MOF powders suspended in organic liquid indicated, under 365 nm irradiation. (b) Height-normalized luminescent spectra of guest-containing MOFs upon excitation at 370 nm. (c) Relationship between the emission energy of guest-containing MOF and the ionization potential of the guest. Reprinted with permission from ref 76. Copyright 2011 Nature Publishing Group.

electronic structure of the luminescent moieties can be systematically varied.⁴⁸ In addition, however, the extent of the interaction

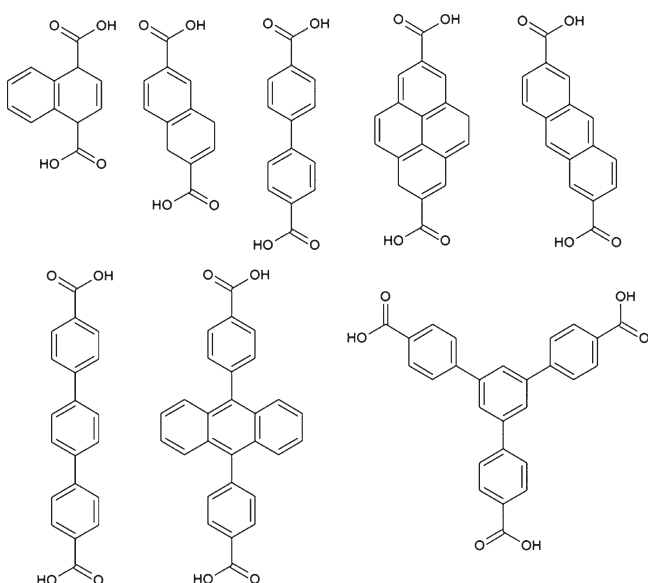


Figure 6. Representative sampling of scintillating linker groups used in MOF synthesis. Reprinted with permission from ref 48. Copyright Elsevier.

among emitting groups can be varied, either by tuning the pore size or by creating interpenetrated structures in which the distance and orientation between crystal lattices differ from those in the noninterpenetrated structure. The IRMOFs provide a particularly interesting isostructural series from this perspective, because both interpenetrated and noninterpenetrated structures incorporating the same linker exist (e.g., IRMOF-9 and IRMOF-10, in which the linker is biphenyldicarboxylate).

MOF-based scintillators were first reported by Doty et al.⁷⁷ Two MOFs incorporating fluorescent stilbene dicarboxylate (SDC) linkers were characterized, one of which has a porous, interpenetrated structure with 3D topology known as Zn₄O-(SDC)₃ (MOF-S1) and the other a nonporous structure consisting of 2D sheets, Zn₃(SDC)₃(DMF)₂ (DMF = *N,N*-dimethylformamide) (MOF-S2). Prior to this work, Bauer et al. showed that fluorescent lifetimes in these materials approach the natural emission lifetime, due to constraining the stilbene group in a relatively rigid trans orientation.⁷⁸ As a result, the non-emissive cis-trans isomerization pathway in stilbene is blocked, increasing the quantum yield. This led to the hypothesis that emission produced by ionizing radiation would have similar properties. Doty et al. confirmed this, demonstrating radioluminescence from 3 MeV protons (Figure 7) and scintillation from alpha particles (Figure 8). Both MOFs exhibit increased fluorescence lifetimes relative to the isolated linker. They are also highly resistant to radiation damage as compared to crystalline organics such as stilbene and anthracene, suggesting that the combination of coordination bonding and relatively large inter-linker distances (>5.5 Å) quenches destructive radical reactions.

Unexpectedly, the radioluminescence of the two stilbene MOFs is significantly red-shifted from their corresponding photoluminescence, falling within the same wavelength region as the neat crystalline linker. The photoluminescence spectra suggest that the extent of intermolecular interaction in the ground state increases as follows: MOF-S1 (49°) ≈ (linker in dilute solution) < MOF-S2 (79°) < SDC₂ (unknown, but likely ~90°). The interaction increases as the angle between aromatic

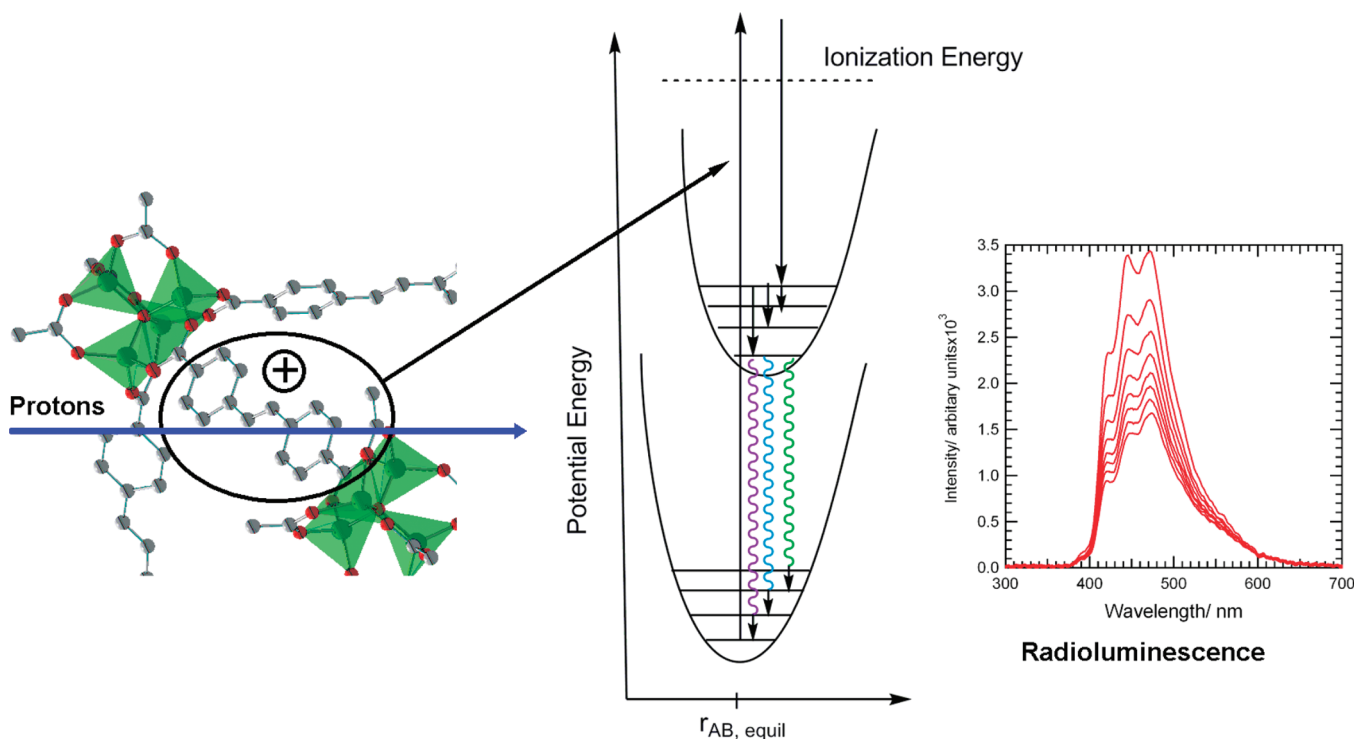


Figure 7. Schematic of the ion-beam-induced luminescence (IBIL) process (using a portion of the MOF-S1 structure for illustration), showing (left) the interaction of a high-energy proton that ionizes the material. The resulting excitation decays (middle) through radiationless pathways (solid arrows) to the lowest-lying singlet excited state of the fluorescent SDC groups, which then decay by emission of photons (wavy arrows) to various ground-state vibrational levels, producing the IBIL luminescence displaying vibronic structure (right). The series of spectra indicate the effect of increasing proton dose, proceeding from 0.4 to 4 MGy for the largest to smallest spectra, respectively.⁷⁷

ring centroids (given in parentheses) increases, while the cofacial distances between the two MOFs are nearly the same. This suggests that ionization causes a structural change in the excited state that increases the electronic overlap between linkers, such that it more closely resembles the local environment in the neat linker. The timing of the emission is structure-dependent as well, as seen in Figure 8. MOF-S1 exhibits a monoexponential decay, while MOF-S2 and SDCH₂ exhibit at least two distinct time scales. These results demonstrate that control over both the electronic structure and the local emitter environment is possible in MOFs. From the point of view of radiation detection, they also suggest that MOFs can be used in detection schemes based on pulse shape discrimination (PSD), a method that distinguishes among particle types by the time dependence of their light output.

Recently, Feng et al.⁴⁸ expanded the concept of using MOF structure to tune luminescence by demonstrating that both dynamic structural changes and incorporation of extrinsic dopants within the MOF pores can be used to create intense new emission. IRMOF-8, comprised of Zn(II) ions and 2,6-naphthalenedicarboxylate linkers (NDC), was used as a platform to probe charge transfer effects induced by photon absorption and high-energy protons. The neat MOF exhibits linker-based (“monomer”) photoluminescence at ~400 nm. In response to 3 MeV protons, however, broad new emission centered at ~475 nm appears, suggesting that an ionization-induced distortion of the structure leads to excimer formation between adjacent NDC linkers (Figure 9). This mechanism was confirmed by comparison with the ion beam-induced luminescence (IBIL) spectrum of the closed and open forms of MIL-69, in which the

linkers are also NDC. Upon removal of solvent, the closed form exhibits new IBIL at 480 nm, which is assigned to excimers that form when NDC linkers become coplanar and separated by only 3.4 Å. Infiltrating IRMOF-8 with the electron donor diethylaniline (DEA) produces a third type of luminescence: broad fluorescence shifted more than 160 nm to the red from neat IRMOF-8 (Figure 9). The broad, structureless nature of this emission suggests formation of an exciplex between the NDC linkers and the DEA. All three emission types (monomer, excimer, and exciplex) are seen in the proton-IBIL of the infiltrated IRMOF-8 complex. These examples further illustrate the remarkable potential of MOFs for “crystal engineering”, in which correlations between structure and properties can be used to design new scintillation materials.

2.3. Interferometry

Other optical methods that have been used for sensing differ from luminescence and solvatochromic measurements in that they do not involve absorption or emission of light by the MOF. Instead, they measure the MOF refractive index (RI), a bulk property (i.e., composite, volume-weighted property of vacuum ($\text{RI} = 1$), empty framework, and adsorbed guest) that changes depending on the amount and RI of the guest. The refractive index is a measure of the interaction of light with polarizable matter, and so increases with increasing number of polarizable electrons and with increasing polarizability of the electrons. Fabry–Pérot interference occurs when incident light undergoes multiple reflections off of two parallel surfaces separated by a distance, l , on the order of the wavelength of light. Transmitted waves that are in phase constructively interfere and produce

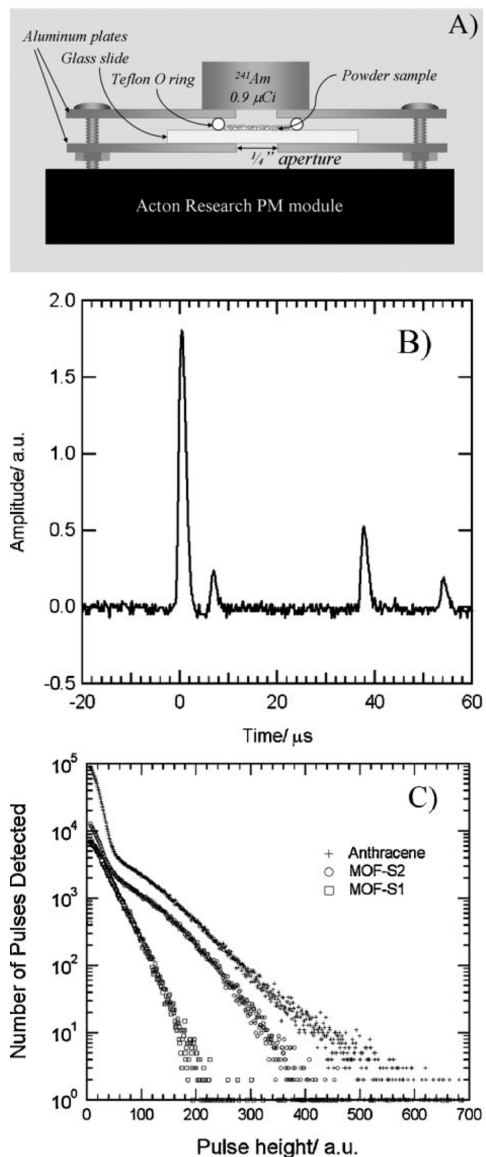


Figure 8. (A) Schematic of experiment used to measure scintillation light output. (B) Photomultiplier (PM) pulses were detected with $2 \mu\text{s}$ shaping time, with the typical oscilloscope trace showing primary pulses at time zero and smaller delayed pulses at various times following the primary pulse. (C) Histogram of scintillation data for anthracene, MOF-S2, and MOF-S1. Reprinted with permission from ref 77. Copyright 2009 Wiley-VCH.

a maximum in the transmission spectrum. The wavelengths at which these maxima occur depend on the refractive index, n , of the medium between the reflective surfaces, as well as the distance between them, l , according to eq 1 where m is an integer and the incident light is assumed to be normal to the surface:

$$m\lambda = 2nl \quad (1)$$

This relationship can be used to detect changes in the refractive index by monitoring shifts of the interference peaks in the transmission spectrum. Lu et al. reported a vapor sensor based on this concept using a thin film of ZIF-8 supported on a transparent glass substrate.⁴⁶ In this case, the reflective surfaces

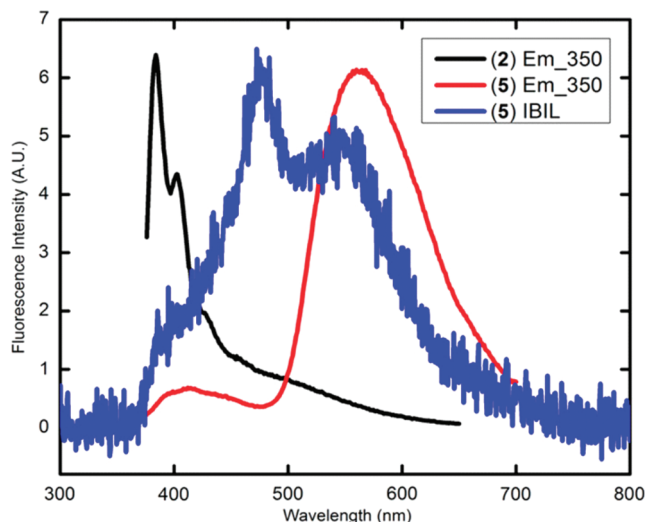


Figure 9. Photoluminescence (red) and IBIL (blue) emission spectra for IRMOF-8 infiltrated with the electron donor diethylaniline (DEA). The monomeric photoluminescence emission for IRMOF-8 (black) is provided for comparison. Reprinted with permission from ref 48. Copyright Elsevier.

are the front and back sides of the MOF film. Because most of the MOF volume is composed of initially vacant pores, sorption of analytes inside of these empty cavities leads to large increases in n .

Unlike fluorescence-based detection schemes, where simple powder or single crystal MOF samples can be used, this measurement requires the MOF to be in thin-film form. The required films were fabricated using a step-by-step method to allow for tuning of the film thickness such that the interference peaks appeared in a convenient region of the spectrum corresponding to the range of a standard UV-vis spectrophotometer. Simply immersing a glass or silicon platform in a solution containing the MOF precursors yielded a 50 nm thick film, presumably via deposition of nanocrystals formed in solution, rather than via direct growth from the glass or silicon platform. The deposition appeared to be self-limiting, with film growth stopping after 30 min. The process could be repeated with fresh precursor solutions, and subsequent repetitions showed a reproducible growth rate of 100 nm per cycle (following the first cycle of 50 nm). Because it requires no surface functionalization, this method of film growth is surface-general while still offering control over thickness. Figure 10A shows films of different thicknesses appearing as different colors due to the thickness-dependence of the reflectance spectra.

Films of approximately 1 μm thickness were used to detect propane in ZIF-8. The resulting increase in refractive index red-shifted the interference peaks by up to 49 nm (see Figure 10B). Perhaps more interesting, however, is that ZIF-8 possesses characteristics potentially useful for selective sensing. The methyl-substituted imidazole strut creates pores that are quite hydrophobic, allowing less hydrophilic molecules to be sensed in the presence of water. For example, the ZIF-8 sensor is unresponsive to water vapor, but ethanol vapor produces a readily detectable shift, as shown in Figure 10C,D. In addition, the small pores ($\sim 3.4 \text{ \AA}$) are useful for sieving of small molecules. In the ZIF-8 sensor, linear *n*-hexane enters the pores and is detected, but the sterically more demanding molecule cyclohexane is excluded.

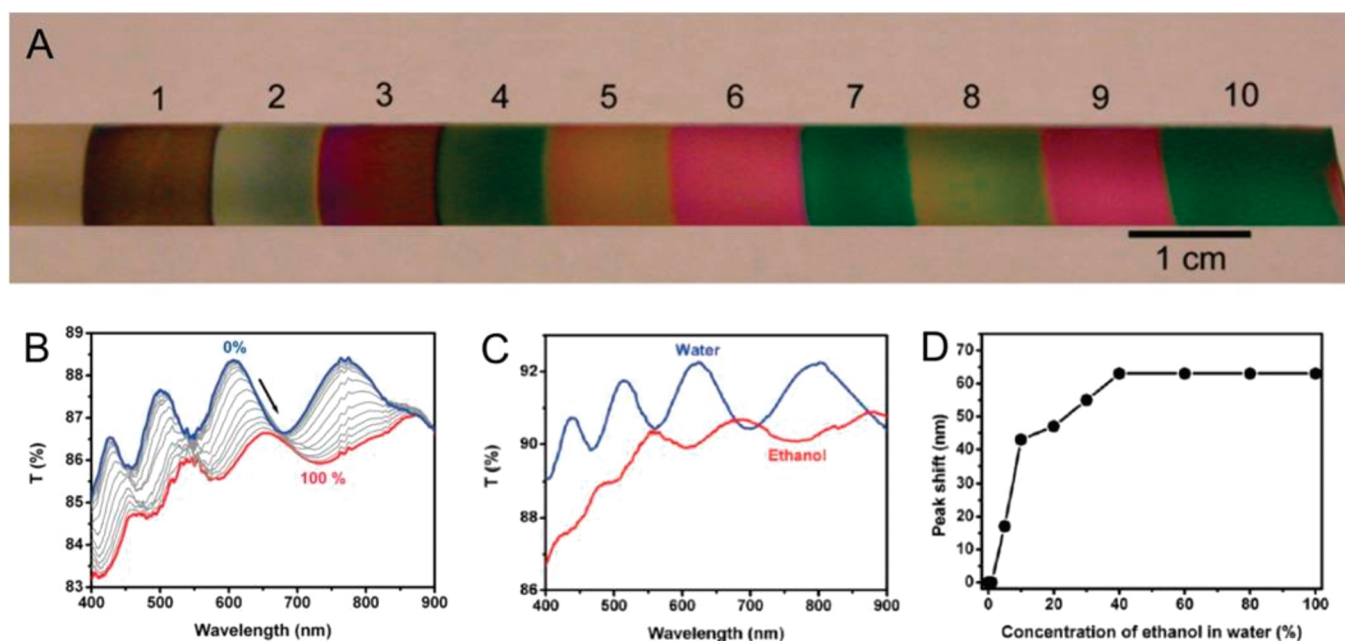


Figure 10. (A) Photo of a series of ZIF-8 films of various thicknesses on Si substrates. UV-vis transmission spectra of ZIF-8 film on glass after exposure to (B) propane vapor of various concentrations from 0% (blue) to 100% (red) and (C) ethanol (red) or water (blue). (D) Interference peak (originally at 612 nm) shift versus ethanol concentration (v/v %) in ethanol/water solutions. Reprinted with permission from ref 46. Copyright 2010 American Chemical Society.

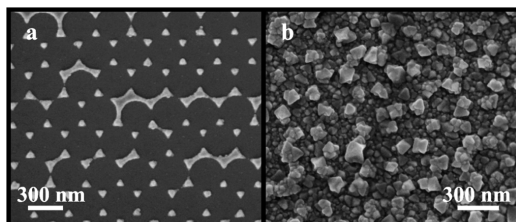


Figure 11. Scanning electron microscopy images of (a) array of Ag nanotriangles on glass substrate and (b) 20 cycles of HKUST-1 grown on an array of Ag nanotriangles. Reprinted with permission from ref 52. Copyright 2010 American Chemical Society.

2.4. Localized Surface Plasmon Resonance

Like interferometry, surface plasmon resonance spectroscopy indirectly detects analytes by measuring changes in MOF RI. When small silver, gold, or copper nanoparticles are irradiated with white light, the conduction band electrons oscillate coherently, a phenomenon known as localized surface plasmon resonance (LSPR).⁷⁸ The frequency of this resonance depends on the RI of the medium surrounding the particles, and changes in this RI can be detected as shifts in the visible extinction spectrum via LSPR spectroscopy. Kreno and co-workers exploited this RI sensitivity to sense sorption of guests inside of a MOF grown on the surface of plasmonic nanoparticles, depicted in Figure 11.⁵²

While LSPR spectroscopy is featured in hundreds of schemes for biological sensing, its utility for sensing gases and vapors has been much more limited. Two primary reasons for this are the need for signal amplification and an inherent lack of specificity. The RIs of different gases differ by only a small amount and are difficult to detect given the resolution of a typical LSPR spectrometer. Furthermore, the plasmonic nanoparticle surface

is inherently nonspecific, and the LSPR frequency is sensitive to all molecules near the particle surface; hence, one cannot tell what molecules are contributing to the signal. Thus, MOFs, which can both concentrate and select for certain analytes, seem a natural complement to this technique.

To demonstrate this principle, Kreno, et al. used a previously reported layer-by-layer technique⁶¹ to grow $\text{Cu}_3(\text{btc})_2(\text{H}_2\text{O})_3$ (btc = benzenetricarboxylate) atop an array of silver nanoparticles fixed on a glass surface. This MOF@Ag array sensor was used to detect CO_2 , as it has been previously demonstrated that $\text{Cu}_3(\text{btc})_2(\text{H}_2\text{O})_3$ readily sorbs CO_2 .⁷⁹ As can be seen in Figure 12A, the shift in the LSPR frequency ($\Delta\lambda_{\text{max}}$) upon dosing CO_2 was measured to be ~ 18 times larger for the MOF@Ag array as compared to a silver particle array lacking the MOF coating. The observed amplification reflects, in part, the relative propensities of the MOF to sorb CO_2 and the purge gas, N_2 (which represents the baseline signal). At ambient pressure, the reported uptake of CO_2 is $\sim 2-4 \text{ mmol g}^{-1}$, as compared to only $\sim 0.2-0.4 \text{ mmol g}^{-1}$ for N_2 .⁸⁰ Thus, there is a significant increase in the MOF refractive index when CO_2 replaces N_2 .

When designing a plasmonic sensor of this type, control over the thickness of the MOF film is paramount. Unlike other techniques that probe the entire sample, LSPR spectroscopy is a surface-sensitive measurement. The refractive index sensitivity is a result of enhanced electric fields at the nanoparticle surface, and these fields decay exponentially, with $1/e$ decay length of ca. 5 nm. Therefore, only molecules within ~ 30 nm of the metal nanoparticle surface are detected. In one respect, this limits the sensitivity of the measurement. The short probe depth of LSPR is also an advantage, however, as it implies that only a very small total amount of analyte is needed to produce the maximum response. The maximum possible response, given an excess of analyte, scales with the surface area of the nanoparticles (i.e., the size of the Ag/MOF interface).

Because ~ 30 nm of the MOF is probed, the ideal films should be at least this thick. Thick films are relatively straightforward to

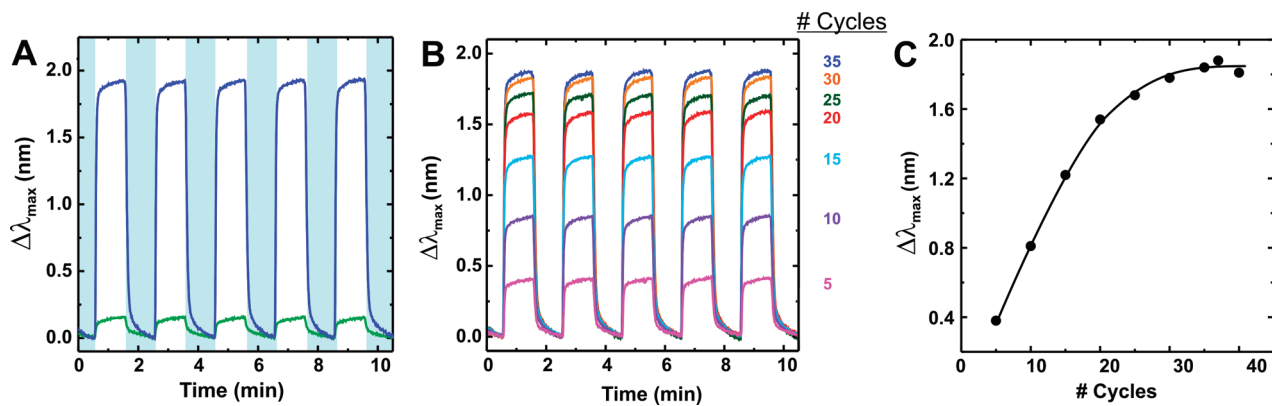


Figure 12. (A) Comparison of bare Ag nanoparticle sensor (green) and MOF-coated sensor (blue) response to CO₂. (B) MOF sensor response to CO₂ for increasing numbers of HKUST-1 growth cycles. In both (A) and (B), CO₂ is dosed for 60 s five times to show reversibility when the sample is purged with N₂. (C) Average peak shift ($\Delta\lambda_{\text{max}}$) as a function of number of growth cycles. Reprinted with permission from ref 52. Copyright 2010 American Chemical Society.

achieve, as most traditional MOF synthetic techniques (i.e., solvothermal) produce crystals with dimensions much larger than this. However, if the MOF film is too thick, the kinetics of analyte diffusion within the film may limit the speed of the sensor response. For this study, the layer-by-layer growth technique gave, in principle, single molecular layer control over film growth. Systematic study of the sensor response as a function of film thickness showed that the response plateaus after $\sim 35\text{--}40$ layers where, presumably, the thickness of the MOF film exceeds the plasmonic probe depth (see Figure 12B,C).

Improvements on this type of sensor will include interfacing plasmonic particles with more chemically selective MOFs. A potential route to increased sensitivity would be to take advantage of resonance effects that amplify the response when the analyte molecule absorption overlaps with the plasmon resonance.⁸¹ Incorporation of metal nanoparticles into MOFs has recently become an active area of research for heterogeneous catalysis. Some have suggested that by including small metal nanoparticles inside of MOFs, one could take advantage of another surface-plasmon-based phenomenon, the surface-enhanced Raman scattering effect.⁸²

2.5. Colloidal Crystals

MOF-containing colloidal crystals (CCs) present another opportunity for optical detection of analytes. Colloidal crystals consist of three-dimensional ordered arrays of submicrometer particles, often formed by the self-assembly of polystyrene or silica microspheres. Because of its periodicity, the CC acts as a diffraction grating for light with wavelengths on the same length scale as the particle size. As such, CCs reflect light at a specific wavelength (stop band) that depends in part on the refractive index of the particles and the medium filling the interstitial spaces, making them versatile refractive index-based sensors. Lu et al. used the layer-by-layer method⁶¹ to grow HKUST-1 in the interstitial spaces between ordered silica microspheres, yielding a composite MOF-silica colloidal crystal (MOF-SCC).⁸³

The wavelength, λ , of the stop band is a function of the microsphere diameter, D , and the refractive index, n , as described by eq 2 for the [111] direction of the CC, assuming normal incidence.

$$\lambda = \frac{2\sqrt{2}}{\sqrt{3}}nD \quad (2)$$

In this case, n is a volume-weighted average of the refractive indices of both the silica microspheres ($n_{\text{SiO}_2} > 1$) and the MOF, where the MOF itself can be considered a combination of the framework volume (n_{fram}) and the empty pore volume (n_{cavity}). Thus, the refractive index of the MOF-SCC composite can be described by eq 3, where f_{SiO_2} and f_{fram} represent the volume fractions of silica and MOF framework in the MOF-SCC, respectively.

$$n = \sqrt{f_{\text{SiO}_2}n_{\text{SiO}_2}^2 + f_{\text{fram}}n_{\text{fram}}^2 + (1 - f_{\text{SiO}_2} - f_{\text{fram}})n_{\text{cavity}}^2} \quad (3)$$

In its dehydrated state, the empty MOF cavity can be represented as vacuum ($n_{\text{cavity}} = n_{\text{vacuum}} = 1$). Subsequent sorption of guests ($n > 1$) increases the effective MOF-SCC refractive index resulting in a stop band red shift.

The HKUST-1 MOF-SCC sensors were tested for both vapors and gases. Figure 13a shows the shifting of the stop band up to ~ 16 nm induced by carbon disulfide adsorption. Because the refractive index change increases with increasing amounts of adsorbed carbon disulfide, the shift also depends predictably on analyte concentration (Figure 13b,c). By converting these stop-band shifts to normalized volume fractions of adsorbates, Lu and co-workers were able to construct adsorption curves on the basis of their optical measurements (Figure 13d). The shapes of these isotherms could be validated by separately quantifying the vapor sorption in HKUST-1 films by quartz crystal microbalance (Figure 13e). Given the ability of HKUST-1 to sorb a wide range of analytes, it is not surprising that the sensor also responded to other vapors including water and ethanol, as well as gases, including argon, carbon dioxide, ethane, ethylene, and ambient air. The stop band shift for the gaseous analytes is depicted in Figure 13f. Shifts in the stop band as small as 0.015 nm were resolvable, yielding limits of detection as low as 2.6, 0.5, and 0.3 ppm for water, carbon disulfide, and ethanol, respectively.

2.6. Impedance Spectroscopy

Studies on chemiresistive metal oxide, solid electrolyte, and metal–oxide–semiconductor field-effect transistor sensors abound in the literature, but MOFs have rarely been utilized for conductivity-based sensing applications. Since the demonstration of a ZnO thin film gas sensor in the early 1960s,⁸⁴ much sensor research has centered on nanoengineering and doping of metal oxides for improved performance. Although semiconducting metal oxides

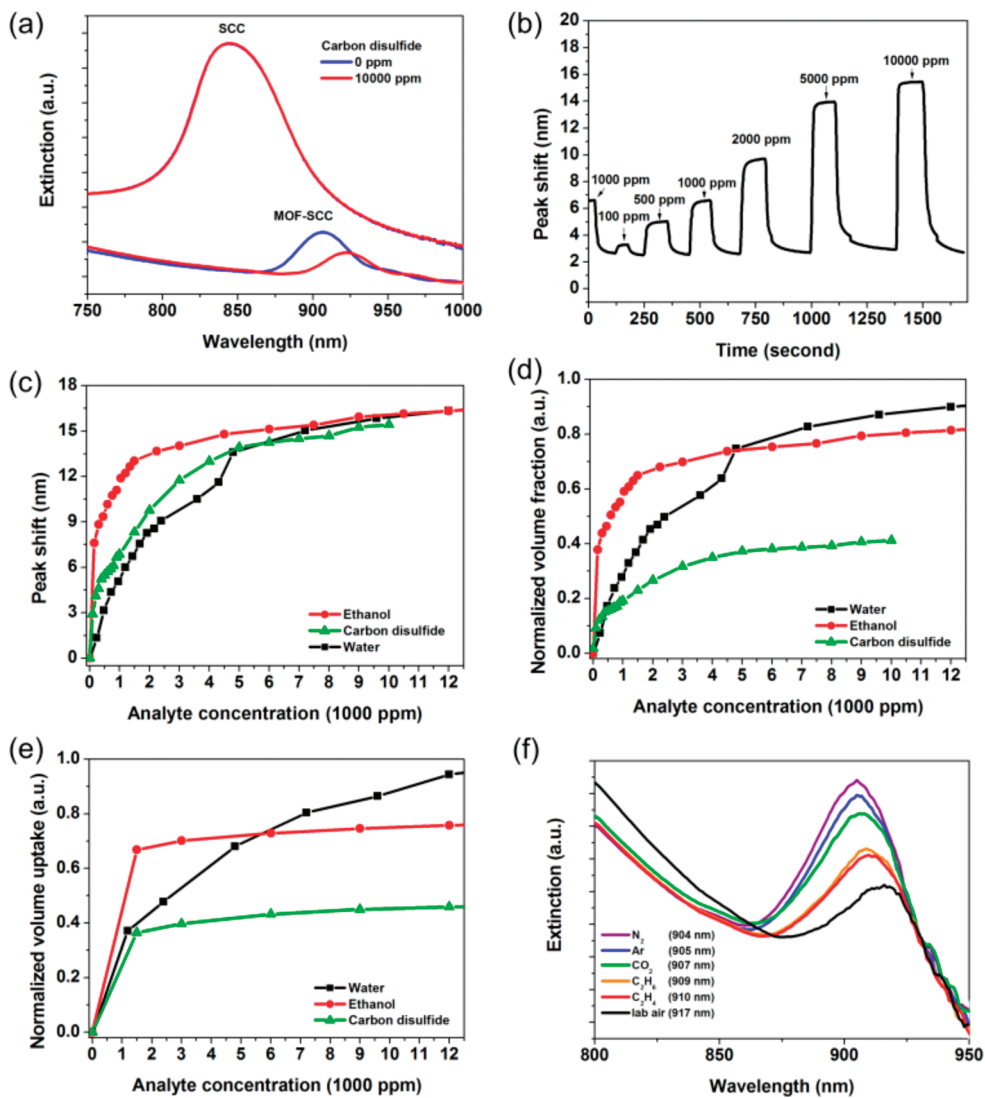


Figure 13. (a) Near-IR extinction spectra of MOF-silica colloidal crystal (MOF-SCC) thin film and unmodified colloidal crystal thin film before and after exposure to 10 000 ppm carbon disulfide (bottom); and (b) responses of MOF-SCC to a series of carbon disulfide vapors of various concentrations versus time. (c) Dependence of stop band peak shift of the MOF-SCC thin film on the vapor concentrations of different solvents; (d) normalized vapor adsorption isotherms of different solvents by MOF-SCC; (e) normalized vapor adsorption isotherms of different solvents by HKUST-1 thin film grown on a quartz crystal microbalance electrode; and (f) near-IR extinction spectra of MOF-SCC thin film on exposure to lab air, argon, nitrogen, carbon dioxide, ethane, and ethylene. Reprinted with permission from ref 83. Copyright 2011 Wiley-VCH.

respond to a wide range of oxidizing and reducing analytes, they suffer from a host of limitations. The mechanism of molecular recognition in these sensors involves the reaction of gases from the atmosphere with oxygen species adsorbed on the oxide surface.⁸⁵ For these processes, the sensors typically must be operated above 200 °C.⁹ In addition, they exhibit long-term baseline drift and cross-sensitivity for different analytes.⁹

Achmann et al. recently adapted this electrical sensing platform to MOF sensors.⁵⁴ In principle, MOFs offer a distinct advantage over oxide films due to their selective sorption capabilities. Furthermore, MOF sorption, and therefore sensing, occurs at low (ambient) temperature.

Achmann et al. screened three different commercially available MOF materials: Al-terephthalate-MOF (Al-BDC), Fe-1,3,5-benzenetricarboxylate (Fe-BTC), and Cu-1,3,5-benzenetricarboxylate (Cu-BTC). Electrical properties of the MOFs were measured in two different configurations pictured in Figure 14.

First, pastes of the respective MOFs were screen printed atop a patterned array of interdigital electrodes. In a second setup, commercially prepared MOF pellets were contacted by metal disk electrodes. In both cases, impedance spectra were measured as the MOF was exposed to various gases and vapors: 10% O₂, 10% CO₂, 1000 ppm C₃H₈, 1000 ppm NO and 1000 ppm H₂, 0–18% ethanol, 1–35% methanol, and water.

Both devices using the Fe-BTC MOF responded reproducibly to water vapor with the absolute value of the complex impedance, |Z|, decreasing linearly with increasing water vapor concentration, c(H₂O), at the lowest measured temperature, 120 °C (see Figure 15). At higher temperatures, however, the sensitivity to changes in water concentration decreased, and the dependence changed to an exponential decay of the following form (values of R provided in Figure 15):

$$|Z| = |Z_0| + A \cdot e^{(-R \cdot c(H_2O))} \quad (4)$$

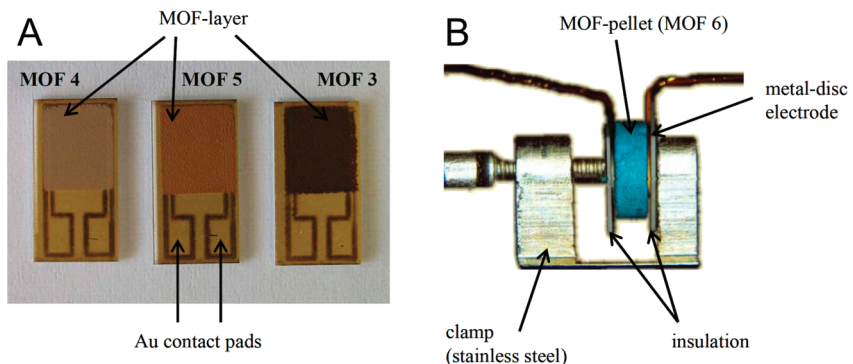


Figure 14. (A) MOF films deposited on interdigital electrodes. (B) MOF pellet pressed between gold disk electrodes. Reprinted with permission from ref 54. Copyright 2009 MDPI AG.

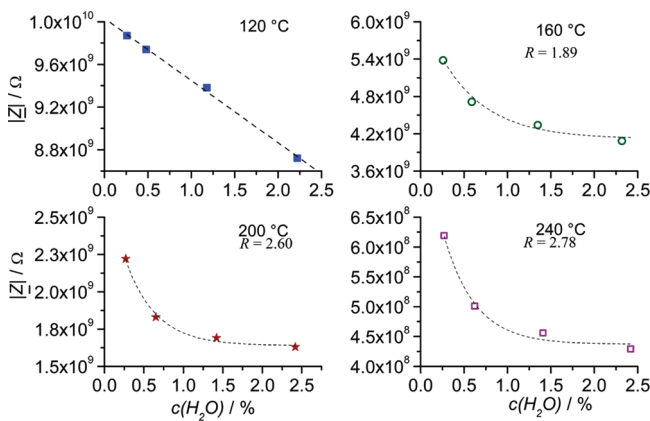


Figure 15. Response curves ($|Z|$ vs H_2O concentration) of a planar Fe-BTC interdigital electrode sensor at different temperatures: 120, 160, 200, and 240 °C. The sensor characteristics changed from a linear dependence at 120 °C to a behavior that can be approximated by exponential decay. Measurement frequency: 1 Hz. Reprinted with permission from ref 54. Copyright 2009 MDPI AG.

The authors attribute this temperature dependence to either faster saturation or more significant desorption as the temperature increases. The sensor responded similarly to ethanol and methanol with sensitivity increasing in the following order: methanol < ethanol < water. Al-BDC also responded to humidity changes, but significant drift of the baseline led to irreproducible measurements. Despite this limitation, Achmann et al. demonstrated that the Fe-BTC sensor can fill a need for humidity sensing where current sensors fail, at water concentrations below 10% and at low temperature.

There are clear advantages of the impedance method in terms of ease of fabrication as compared to other sensing modalities. Because the MOF is coated onto the electrode surface as a paste or pressed into a freestanding pellet, it can be synthesized in bulk rather than grown on a surface. Thus, this is truly a MOF-general approach. Unfortunately, none of the tested materials responded to any of the purely gas-phase analytes. Although some MOF materials have certainly exhibited high sorption capacities for gases, it is unlikely that they cause significant changes in MOF electrical properties and therefore cannot be readily detected by this method. Rather, impedance spectroscopy will likely be limited to solvent and vapor sensing. More highly conducting MOFs have recently been under development for other applications,⁵³ but may prove good candidates for impedance-based sensing due to their guest-dependent conductivity.

2.7. Electromechanical Sensors

Electromechanical devices such as the quartz crystal microbalance (QCM),⁸⁶ surface acoustic wave sensors (SAWS),⁸⁶ and microcantilevers (MCL)⁸⁷ are logical starting points for using MOFs in chemical sensing applications. Although these devices employ different transduction mechanisms, in each case signal detection requires the analyte to be adsorbed onto the surface of the sensor. Very high detection sensitivities are possible (femtogram levels in MCL); however, a coating of some type is required to activate this sensitivity and impart specificity for a specific analyte. Historically, organic polymers have served this purpose, although there are also examples in which zeolites and other materials were used.^{88–91} As discussed above, the extremely high surface areas and tunable pore environments of MOFs offer clear advantages in this regard.

2.7.1. Quartz Crystal Microbalance. These devices detect analytes by sensing small changes in the frequency of a resonant vibration propagating perpendicular to the surface of a quartz crystal.⁸⁶ As compared to other mass-based detection methods, their sensitivity is relatively low (~ 1 ng detection limit); however, they are straightforward to use and provide a useful platform for measuring adsorption isotherms and surface kinetics, as well as sensing. For example, this technique has been used to evaluate the potential of zeolite thin films for humidity and organic vapor sensing.^{92,93} A typical QCM-electrode consists of a circular quartz plate with a diameter of 15 mm and thickness of 1 mm. Most small molecules do not bind strongly to quartz surfaces, necessitating the use of a coating to provide sensitivity and selectivity. However, MOF thin films can be deposited on QCMs with relative ease because their hydroxylated surface provides reactive sites for binding linkers and metal ions.

Water sorption studies, using self-assembled monolayers (SAMs) to attach the MOF to the QCM electrodes, provide the first example of MOF-based sensing using these devices. MOFs are attractive for humidity sensing, which has many domestic and industrial applications,⁹⁴ due to their large pore volumes and high surface areas. Water uptake as high as 41 wt % has been reported.⁵⁵ In addition, their much higher thermal stability relative to organic polymers allows them to be baked at high temperature to remove adsorbed water quickly and regenerate the sensor. Biemmi et al. demonstrated selective growth of $\text{Cu}_3(\text{BTC})_2$ (Cu-BTC; also known as HKUST-1) on functionalized QCM gold electrodes to evaluate the sorption properties of MOF thin films.⁵⁵ The preparation of the MOF thin film was achieved by direct growth on a 11-mercaptopoundecanol SAM. When these films (film mass ($45\text{--}71$) $\times 10^{-6}$ g cm^{-2}) were

exposed to water, the QCM revealed a clear mass uptake, indicating loading of the MOF with water molecules. As a result, the water sorption properties of the deposited MOF material could be studied in a rather straightforward fashion (Figure 16). Ameloot et al. also demonstrated water vapor detection with a MOF-coated QCM, using electrochemically synthesized Cu-BTC films grown directly on the device.⁵⁶ They showed that changes in relative humidity can be monitored and a highly reproducible signal occurs upon cycling between dry and water-containing nitrogen flows (Figure 17). The water sorption capacity of the films was found to be 25–30 wt %.

Diffusion constants for small molecules within porous MOFs can be measured using a MOF-coated QCM. Zybaylo et al. deposited a highly ordered thin film of Cu-BTC on the QCM gold electrode using a liquid-phase epitaxy (LPE) method.³⁸ The diffusion constant of pyridine was obtained by measuring the time-dependence of the mass uptake. The homogeneous nature of the MOF thin films, together with their well-defined thickness, allowed the QCM data to be modeled assuming Fickian diffusion and a hopping mechanism. For pyridine, a diffusion coefficient at room temperature of $1.5 \times 10^{-19} \text{ m}^2 \text{ s}^{-1}$ was obtained. The corresponding binding energy of pyridine to the exchangeable

Cu(II) sites in Cu-BTC was determined to be 18 kcal mol⁻¹, in good agreement with the results of ab initio quantum chemistry calculations.³⁸

2.7.2. Surface Acoustic Wave Devices. Surface acoustic wave (SAW) sensors⁸⁷ are robust devices that have been used extensively for chemical sensing. As such, they are also useful for screening mass uptake by materials such as MOFs by depositing them on the sensor surface. Gas adsorption is detected by measuring the frequency shift (typically a decrease) of acoustic waves traveling parallel to the surface that are generated by an oscillator (usually quartz) vibrating in the 25–500 MHz range.

Recently, Robinson and co-workers reported humidity detection over a very broad concentration range using SAWs coated with Cu-BTC (shown in Figure 18).⁹⁵ The MOF film was grown directly on the quartz of 96.5 MHz devices without an intervening SAM, using the layer-by-layer (LBL) growth method developed by Fischer et al.⁶¹ Frost points (FP) as low as -70 °C and as high as 10 °C (2.6 ppmv and 12 300 ppmv at an atmospheric pressure of 625 Torr, respectively) can be detected. The response is fast (seconds) and reproducible. These results demonstrate 3 orders of magnitude better response to humidity using HKUST-1 as compared to the same coating on QCMs.^{55,56,94,96} The detection range also compares favorably with field-effect transistor sensors coated with porous alumina, which have demonstrated 1 ppmv sensitivity.⁹⁷

The dependence of SAW sensor response on film thickness was also determined. Cu-BTC layers varying from 75 to 350 nm were grown using 10, 20, 30, 40, 50, 60, and 100 LBL cycles. The response to water vapor as a function of the number of coating cycles, shown in Figure 19, indicates that there is an optimal thickness, above which sensor response saturates. For coatings of 40–100 cycles, corresponding to 150, 175, 200, and 350 nm film thicknesses, respectively, the response to low humidity (-50 °C to -40 °C FP) did not appreciably increase after 50 cycles. This is evidently due to poor coupling of the portions of the film far from the SAW surface to the acoustic waves. SAWs with 10–30 coating cycles are not shown here as their responses were significantly lower.

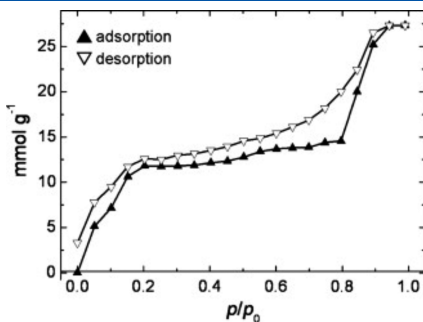


Figure 16. Water adsorption isotherm recorded at 294 K using a QCM setup with a film of $\text{Cu}_3(\text{BTC})_2$. Reprinted with permission from ref 55. Copyright 2008 Elsevier.

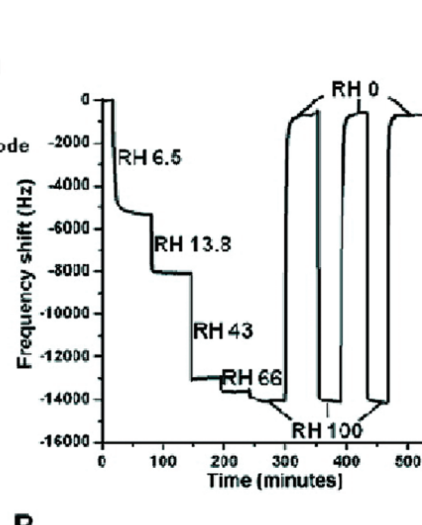


Figure 17. Electrochemically grown $[\text{Cu}_3(\text{BTC})_2]$ coatings in QCM measurement of water adsorption. (A) Schematic representation of the detector configuration. (B) Signal induced by adsorption of water from nitrogen streams at different relative humidity values, illustrating sensor reversibility and reproducibility. Reprinted with permission from ref 56. Copyright 2009 American Chemical Society.

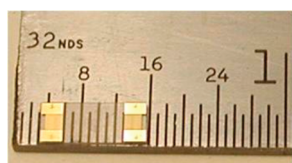


Figure 18. A close-up of a SAW sensor.

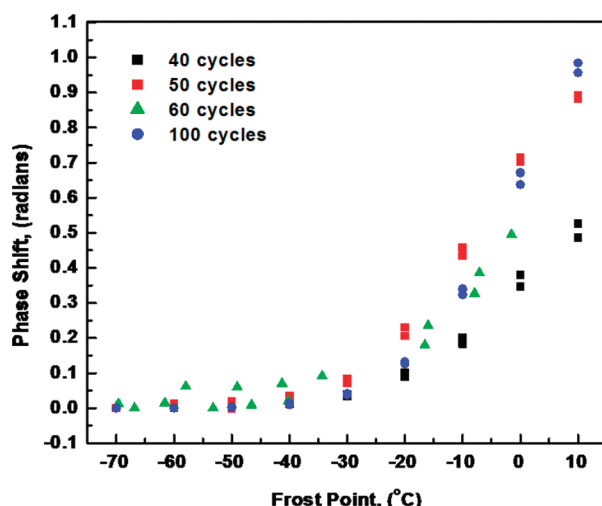


Figure 19. Response of $\text{Cu}_3(\text{BTC})_2$ SAWs with different number of coating cycles to various humidity steps. Reprinted with permission from ref 95. Copyright 2011 Material Research Society.

2.7.3. Microcantilevers. Microcantilevers (MCL) detect the presence of analyte(s) by one of two transduction mechanisms: modification of the cantilever oscillation frequency as a result of mass uptake (dynamic mode) and strain-induced bending (static deflection mode).⁸⁷ In either case, MOF thin films would provide a high surface area that effectively acts as a concentrator for low-concentration analytes. In dynamic mode, changes in sensor oscillation frequency are typically detected optically, while in static mode, adsorption produces strain at the coating–MCL interface, causing deflection of the cantilever beam that can be detected either optically or by using a built-in piezoresistive sensor. An example of a static microcantilever design is shown in Figure 20. In devices of this type, beam displacements $<1\text{ nm}$ can be detected using MOF-coated devices.^{44,98}

The structural flexibility of MOFs is an advantage for chemical detection using static MCL, because even small changes in unit cell dimensions can result in large tensile or compressive stresses at the interface between the cantilever and a MOF thin film. Kitagawa and others have shown that very large changes in unit cell volumes are possible,^{99,100} suggesting that an exquisitely sensitive MOF detector could be fabricated on the basis of this concept. For example, MIL-88 undergoes a 23% change in its unit cell volume upon removal of guest solvent molecules.⁹⁹ Stress-induced chemical detection was demonstrated using a Cu-BTC thin film integrated with a MCL. Cu-BTC does not exhibit very large adsorption-induced structural changes; removal of the coordinated waters changes the unit cell dimension of this cubic MOF by only 0.12 \AA .¹⁰¹ Nevertheless, MCL responses with the MOF both hydrated and dehydrated are detectable. The dehydrated state was achieved by heating the device to $40\text{ }^\circ\text{C}$ under flowing N_2 , which removes physisorbed water within the pores,

but leaves intact the water molecules coordinated to the exchangeable Cu(II) sites. In its hydrated state, the MOF-coated MCL responds rapidly and reversibly to gas-phase water, methanol, and ethanol, while no response to N_2 , O_2 , or CO_2 is observed (Figure 21). In contrast, when the MOF layer is dehydrated, the sensor responds to CO_2 , suggesting that hydrophilic molecules such as alcohols can displace physisorbed water, whereas weakly interacting gases such as CO_2 require open volume to be detected. These results show that the energy of molecular adsorption, which causes slight distortions in the MOF crystal structure, can be converted to mechanical energy to create highly responsive, reversible, and selective sensor.

While these results are very promising, it is clear that to maximize sensitivity, more needs to be known concerning the influence of MOF mechanical properties and the interaction of these layers with the device. To this end, Lee et al. modeled a MOF-coated MCL to determine the effects of the Young's modulus of the MOF and the composition and thickness of the top dielectric layer, to which the MOF film is attached.⁹⁸ COMSOL modeling of the electromechanical behavior of the cantilever beam shows that sensitivity improves by changing the dielectric film from silicon nitride to silica, which has a lower Young's modulus. The model also predicts that n-type silicon, oriented in the (010) direction of the (100) wafer, has the greatest sensitivity. As was seen above for MOF-coated SAWs, the MCL response increases with MOF thickness. However, it reaches a maximum at $\sim 800\text{ nm}$. This is much thicker than observed for MOF-coated SAWs, suggesting that MCL is potentially much more sensitive than SAWs (in general, this is the case). However, the COMSOL model assumes a completely dense material and does not account for the relatively weak and thus flexible linkages within the framework. Therefore, it is likely that MCL response will saturate at much a lower coating thickness. The response can be improved by increasing the MOF Young's modulus. Recent nanoindentation measurements and modeling indicate that MOFs are stiffer (i.e., higher Young's modulus) than many organic polymers and in a few cases approach the softer metals.¹⁰² Flexibility in this regard is limited, however, because factors such as pore size and linker type that influence mechanical properties are also the synthetic handles used to tune selectivity. Nevertheless, this modeling provides much useful insight into the design of MOFs for sensing and their proper integration with electromechanical devices.

In each of these sensor types, the MOF film must be tightly attached to the device surface to obtain good sensitivity. Film morphology may also influence sensitivity, but this has yet to be investigated. We expect that dense, pinhole-free films with thicknesses on the order of 100 nm will provide sufficient analyte adsorption to be detected by QCM, SAW, and MCL devices with adequate response times. Currently available methods for growing MOF films produced polycrystalline films, which if they are very rough will scatter acoustic waves to a greater extent than amorphous films that lack grain boundaries, reducing the sensitivity of SAW and QCM devices. Very smooth Cu-BTC films can be grown on substrates coated with thiol-based SAMs as the attachment layer; rms roughness $\leq 5\text{ nm}$ is achievable, which corresponds to approximately two unit cells.¹⁰³ However, the roughness on other surfaces can be considerably greater.⁶⁴ It is therefore clear that a need exists for versatile coating methods in which both film thickness and morphology can be controlled. MOF film growth has been recently reviewed,^{59,60,104}

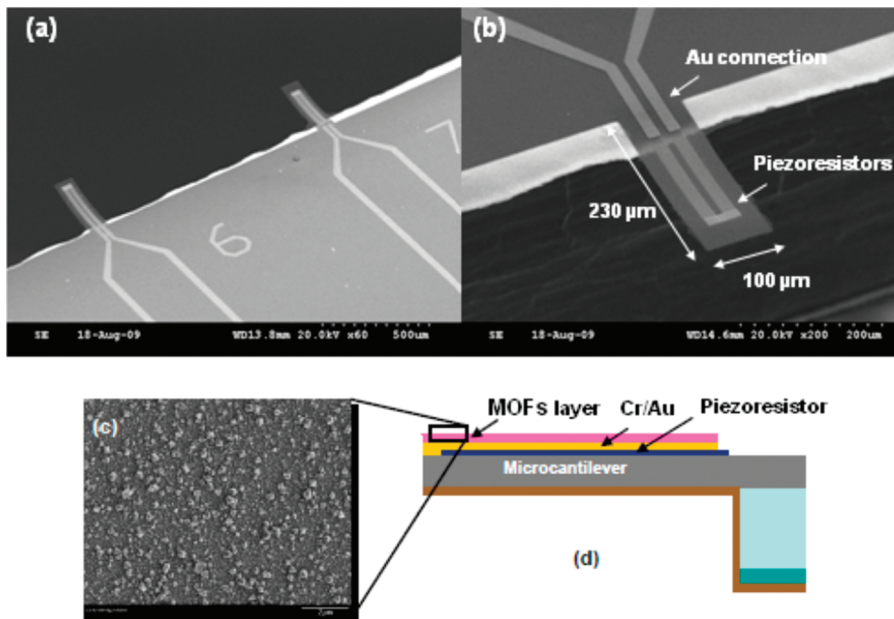


Figure 20. SEM of piezoresistive microcantilever before MOFs deposition. (a) Each microcantilever array consisted of 10 cantilevers. (b) The cantilever width is 100 μm , and the resistors are 20 μm wide. The cantilever length is 220 μm , and the resistor is 185 μm . (c) SEM micrograph of HKUST-1 on Au. (d) Schematic diagram of piezoresistive microcantilever to assemble with MOFs. Reprinted with permission from ref 98. Copyright 2010 SPIE.

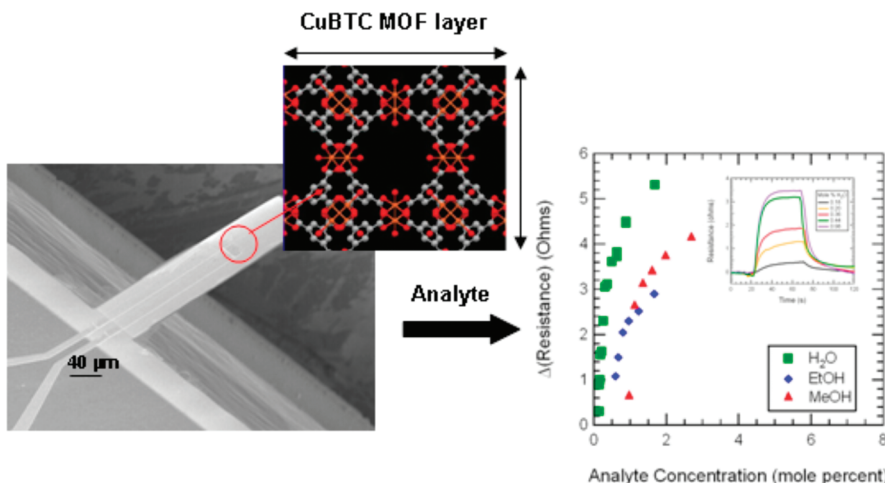


Figure 21. Illustration of a microcantilever coated with Cu-BTC. The resistance change versus analyte concentration, expressed as a percentage of the total gas flow (balance N_2 ; 298 K and 1 atm), is shown. Inset shows the temporal response to H_2O vapor. Reprinted with permission from ref 44. Copyright 2008 American Chemical Society.

highlighting that this aspect of MOF science is still in its infancy, with coating methods developed for only a handful of MOFs.

3. CONCLUSIONS AND FUTURE OUTLOOK

MOF sensors have shown excellent potential for detecting a range of organic molecules and ions (as well as detecting radiation), but there is much room for improvement. Literature reports are dominated by studies of luminescent MOFs fabricated by traditional methods. However, significant progress has been made beyond this somewhat limited approach due to two advances.

First, the employment of other signal transduction methods has provided access to nonluminescent MOFs, which otherwise display no observable sensing signal. Many of the methods presented here, including interferometry, colloidal crystals, LSPR, QCM, SAW, and microcantilever devices, can be applied to any MOF material without concern for the properties or structure of specific MOF materials. Furthermore, MEMS devices, in particular, hold great promise for the development of miniaturized, portable sensors.

Second, the recent proliferation of MOF thin-film growth techniques has been essential in enabling the fabrication of these devices. When MOF materials could only be synthesized by solvothermal methods that produced free-standing crystals, signal

transduction was limited to only a few approaches. As we implement new techniques to grow these structures on substrates, we can not only access different length scales of MOF structures, but also create good interfaces between MOFs and support surfaces.

Despite the growing catalogue of MOF materials, the goal of highly selective recognition remains unrealized for most analytes. It is unlikely that a high level of specificity can be achieved by shape or size selectivity alone. In certain cases, clever design tricks may be used to install sophisticated recognition elements into MOFs. For example, one could imagine a chiral framework that recognizes only one enantiomer in a mixture, and, indeed, some examples of preferential (albeit, not exclusive) enantiomer sorption have been reported.¹⁰⁵ MOFs containing exposed metal centers can bind certain gas molecules while remaining blind to other atmospheric interferents.^{106,107}

While exceptions doubtless will be found, routinely designing or discovering MOF materials that respond very selectively only to a single analyte will likely prove difficult or impossible for the foreseeable future. A seemingly attractive alternative that has been fairly extensively explored with chemosensory polymers would be to construct an array-based device containing several distinct materials (in this case, MOFs) that collectively act as a chemical nose.^{108–110} In principle, each analyte interacts with the series differently to produce a unique fingerprint. In practice, the effectiveness of the approach is somewhat limited because the “unique fingerprint” changes with analyte concentration. Additionally, the array or nose addresses only the problem of identification, and not the problem of signals from interferants. It is also important to recognize that gas or vapor sorption by a conventional polymer is mainly an issue of solubility. For the most part, analyte size and shape are unimportant. Furthermore, unlike in the case of MOFs, strategically positioning multiple analyte-recognition functionalities within uniform and well-defined cavities is not possible with conventional polymers. It seems unlikely, therefore, that the array or nose approach will prove as useful for MOFs as it has for other candidate chemosensory materials.

A better approach may be computational ranking and screening of MOFs, where the library of materials can be generated either by data mining (e.g., by examining the several thousand crystal structures of potentially porous coordination polymers already present in the Cambridge Structural Database) or by combining linkers and nodes in silico to create both existing and hypothetical MOFs. While high throughput screening of structurally and electrostatically simple molecules such as methane can likely readily be accomplished,¹¹¹ larger molecules possessing more degrees of freedom of motion (e.g., octane) or molecules presenting more complex electrostatics (e.g., SO₂) require more complex simulations that necessarily will be slower. Sorption simulations involving MOFs that present open metal sites that can engage in weak bonding interactions with a target analyte will typically require computationally expensive, quantum chemical calculations to yield reliable predictions. Widespread implementation of high throughput screening of MOFs for highly specific analyte adsorption, therefore, will likely become practical only when significantly greater computational power becomes routinely available and/or when reliable approximate methods for handling more complex molecule/MOF interactions have been devised and validated.

Despite these caveats, a recent computational screening investigation of a comparatively limited library of MOFs provides reasons to be optimistic.⁴⁷ In this study, it proved possible to identify MOFs capable of discriminating between relatively similar molecules (e.g., xylenes and TNT). Additionally, a recent computational study by Ryan and co-workers of eight MOFs led

to the identification of a MOF predicted to show a strong preference for sorption of xenon versus krypton.⁴

Finally, another promising concept for improving selective detection is to couple MOFs with vibrational spectroscopy or another analytical technique that provides a molecular fingerprint. While infrared (and to a lesser extent Raman) spectroscopy has been used to characterize MOFs, the observation/characterization of guest molecules inside of MOFs via these methods has been largely underutilized.^{112–114} Vibrational spectroscopy is capable of detecting analytes without the assistance of a sorbent; however, a MOF could greatly improve the limit of detection via molecule-specific preconcentration, especially if preconcentration occurs proximal to (i.e., within a few nanometers of) a material such as nanostructured gold or silver that can support SERS (surface-enhanced Raman scattering).

AUTHOR INFORMATION

Corresponding Author

*Phone: (925) 294-2895 (M.A.); (847) 491-3504 (J.T.H.). E-mail: mdallen@sandia.gov (M.A.); j-hupp@northwestern.edu (J.T.H.).

BIOGRAPHIES



Lauren E. Kreno received a B.A. in chemistry from Cornell University in 2008. She is currently pursuing a Ph.D. in inorganic chemistry at Northwestern University in the research groups of Joseph Hupp and Richard Van Duyne. Her work focuses on utilizing the optical properties of plasmonic nanoparticles as well as the sorption properties of porous metal–organic framework materials to develop chemical sensors.



Kirsty Leong received her B.S. in chemistry from the University of California at Riverside and her Ph.D. in analytical

chemistry from the University of Washington working under Professor Alex K.-Y. Jen. Her thesis work on plasmonic hybrid systems focused on surface-enhanced fluorescence of nanoparticles and quantum dots. She is currently a postdoctoral researcher at Sandia National Laboratories. Her research interests include the synthesis and characterization of crystalline porous materials, and materials/device fabrication for applications in radiation detection, sensing, and solar cells.



Omar K. Farha is currently a research associate professor in the Chemistry Department at Northwestern University. He was a National Science Foundation Fellow during his Ph.D. studies. He earned his Ph.D. in Chemistry from the University of California, Los Angeles, under the direction of Prof. M. Frederick Hawthorne. He carried out postdoctoral studies with Prof. Joseph T. Hupp at Northwestern University's Institute for Nanotechnology. His current research focuses on the rational design of metal–organic framework and porous-organic polymer materials for sensing, catalysis, gas storage, and gas and chemical separations.



Mark Allendorf is a Distinguished Member of the Technical Staff at Sandia National Laboratories in Livermore, CA. He received his Ph.D. in inorganic chemistry from Stanford University in 1986. His current research interests include nanoporous materials for chemical and radiation sensing, metal hydrides for hydrogen storage, and high-temperature chemistry for solar-driven fuels production. Dr. Allendorf is a Fellow of The Electrochemical Society and formerly that organization's president. He is the author of over 120 technical papers and the editor of seven books.



Richard P. Van Duyne is Charles E. and Emma H. Morrison Professor of Chemistry and of Biomedical Engineering at Northwestern University. He received a B.S. (1967) at the Rensselaer Polytechnic Institute and a Ph.D. (1971) at the University of North Carolina, Chapel Hill, both in chemistry. Van Duyne is a member of the National Academy of Sciences and the American Academy of Arts and Sciences. He is known for the discovery of surface-enhanced Raman spectroscopy (SERS), the invention of nanosphere lithography (NSL), and the development of ultrasensitive nanosensors based on localized surface plasmon resonance (LSPR) spectroscopy.



Joseph Hupp joined Northwestern University's Department of Chemistry in 1986 as an assistant professor. Currently he holds the title of Morrison Professor. Additionally he is a Senior Science Fellow at Argonne National Laboratory where he is affiliated with the Materials Science Division and the Chemical Science and Engineering Division. He also serves as an Associate Editor for the *Journal of the American Chemical Society*. He earned a B.S. degree from Houghton College and a Ph.D. from Michigan State, and pursued postdoctoral research at the University of North Carolina. At NU he has mentored approximately 110 Ph. D. students, postdoctoral researchers, and visiting scholars. His current research interests center largely on the design, synthesis, characterization, and fundamental investigation of new materials for energy-relevant applications, with much of the work involving metal–organic framework or porous-organic polymer materials. Of particular interest are new materials and molecules that can facilitate light-to-electrical energy conversion, light-to-chemical energy conversion, chemical separations, chemical catalysis, carbon capture, hydrogen storage, or chemical sensing. His research is described in 370 scientific articles.

ACKNOWLEDGMENT

The Northwestern group gratefully acknowledges the Defense Threat Reduction Agency (grant no. HDTRA1-09-1-0009) and the National Defense Science and Engineering Graduate Fellowship program (fellowship for L.E.K.) for support of their own research on MOFs as chemical sensors. The Sandia group gratefully acknowledges the support of the U.S. Department of Energy Office of Proliferation Detection Advanced Materials Program and the Sandia Laboratory Directed Research and Development Program. Sandia National Laboratories is a multi-program laboratory managed and operated by Sandia Corporation, a wholly owned subsidiary of Lockheed Martin Corporation, for the U.S. Department of Energy's National Nuclear Security Administration under contract DE-AC04-94AL85000.

REFERENCES

- (1) Tranchemontagne, D. J.; Mendoza-Cortes, J. L.; O'Keeffe, M.; Yaghi, O. M. *Chem. Soc. Rev.* **2009**, *38*, 1257.
- (2) Wang, Z.; Cohen, S. M. *Chem. Soc. Rev.* **2009**, *38*, 1315.
- (3) Farha, O. K.; Yazaydin, A. O.; Eryazici, I.; Malliakas, C. D.; Hauser, B. G.; Kanatzidis, M. G.; Nguyen, S. T.; Snurr, R. Q.; Hupp, J. T. *Nat. Chem.* **2010**, *2*, 944.
- (4) Ryan, P.; Farha, O. K.; Broadbelt, L. J.; Snurr, R. Q. *AIChE J.* **2011**, *57*, 1759.
- (5) Collins, D. J.; Zhou, H.-C. *J. Mater. Chem.* **2007**, *17*, 3154.
- (6) Li, J.-R.; Ma, Y.; McCarthy, M. C.; Sculley, J.; Yu, J.; Jeong, H.-K.; Balbuena, P. B.; Zhou, H.-C. *Coord. Chem. Rev.* **2011**, *255*, 1791.
- (7) Li, J.-R.; Kuppler, R. J.; Zhou, H.-C. *Chem. Soc. Rev.* **2009**, *38*, 1477.
- (8) Lee, J.; Farha, O. K.; Roberts, J.; Scheidt, K. A.; Nguyen, S. T.; Hupp, J. T. *Chem. Soc. Rev.* **2009**, *38*, 1450.
- (9) Capone, S.; Forleo, A.; Francioso, L.; Rella, R.; Siciliano, P.; Spadavecchia, J.; Presicce, D. S.; Taurino, A. M. *J. Optoelectron. Adv. Mater.* **2003**, *5*, 1335.
- (10) Cavka, J. H.; Jakobsen, S.; Olsbye, U.; Guillou, N.; Lamberti, C.; Bordiga, S.; Lillerud, K. P. *J. Am. Chem. Soc.* **2008**, *130*, 13850.
- (11) Farha, O. K.; Spokoyny, A. M.; Mulfort, K. L.; Hawthorne, M. F.; Mirkin, C. A.; Hupp, J. T. *J. Am. Chem. Soc.* **2007**, *129*, 12680.
- (12) Allendorf, M. D.; Bauer, C. A.; Bhakta, R. K.; Houk, R. J. T. *Chem. Soc. Rev.* **2009**, *38*, 1330.
- (13) Cui, Y.; Yue, Y.; Qian, G.; Chen, B. *Chem. Rev.* [online early access]. DOI: 10.1021/cr200101d. Published online: Jun 21, 2011; <http://dx.doi.org/10.1021/cr200101d> (accessed Aug 13, 2011).
- (14) Rocha, J.; Carlos, L. D.; Paz, F. A. A.; Ananias, D. *Chem. Soc. Rev.* **2011**, *40*, 926.
- (15) Smith, P. A.; Koch, D.; Hook, G. L.; Erickson, R. P.; Jackson Lepage, C. R.; Wyatt, H. D. M.; Betsinger, G.; Eckenrode, B. A. *TrAC, Trends Anal. Chem.* **2004**, *23*, 296.
- (16) Gu, Z.-Y.; Wang, G.; Yan, X.-P. *Anal. Chem.* **2010**, *82*, 1365.
- (17) Dincă, M.; Long, J. R. *J. Am. Chem. Soc.* **2005**, *127*, 9376.
- (18) Eddaoudi, M.; Kim, J.; Rosi, N.; Vodak, D.; Wachter, J.; O'Keeffe, M.; Yaghi, O. M. *Science* **2002**, *295*, 469.
- (19) Farha, O. K.; Malliakas, C. D.; Kanatzidis, M. G.; Hupp, J. T. *J. Am. Chem. Soc.* **2009**, *132*, 950.
- (20) He, H.; Yuan, D.; Ma, H.; Sun, D.; Zhang, G.; Zhou, H.-C. *Inorg. Chem.* **2010**, *49*, 7605.
- (21) Ma, S.; Sun, D.; Ambrogio, M.; Fillinger, J. A.; Parkin, S.; Zhou, H.-C. *J. Am. Chem. Soc.* **2007**, *129*, 1858.
- (22) Shekhah, O.; Wang, H.; Paradinas, M.; Ocal, C.; Schupbach, B.; Terfort, A.; Zacher, D.; Fischer, R. A.; Wöll, C. *Nat. Mater.* **2009**, *8*, 481.
- (23) Zhang, J.; Wojtas, L.; Larsen, R. W.; Eddaoudi, M.; Zaworotko, M. J. *J. Am. Chem. Soc.* **2009**, *131*, 17040.
- (24) Lun, D. J.; Waterhouse, G. I. N.; Telfer, S. G. *J. Am. Chem. Soc.* **2011**, *133*, 5806.
- (25) Deshpande, R. K.; Minnaar, J. L.; Telfer, S. G. *Angew. Chem., Int. Ed.* **2010**, *49*, 4598.
- (26) Farha, O. K.; Mulfort, K. L.; Hupp, J. T. *Inorg. Chem.* **2008**, *47*, 10223.
- (27) Lin, X.; Blake, A. J.; Wilson, C.; Sun, X. Z.; Champness, N. R.; George, M. W.; Hubberstey, P.; Mokaya, R.; Schröder, M. *J. Am. Chem. Soc.* **2006**, *128*, 10745.
- (28) Wang, Z.; Cohen, S. M. *J. Am. Chem. Soc.* **2007**, *129*, 12368.
- (29) Gadzikwa, T.; Farha, O. K.; Mulfort, K. L.; Hupp, J. T.; Nguyen, S. T. *Chem. Commun.* **2009**, *3720*.
- (30) Hwang, Y. K.; Hong, D.-Y.; Chang, J.-S.; Jhung, S. H.; Seo, Y.-K.; Kim, J.; Vimont, A.; Daturi, M.; Serre, C.; Férey, G. *Angew. Chem., Int. Ed.* **2008**, *47*, 4144.
- (31) Hinks, N. J.; McKinlay, A. C.; Xiao, B.; Wheatley, P. S.; Morris, R. E. *Microporous Mesoporous Mater.* **2010**, *129*, 330.
- (32) Bourrelly, S.; Llewellyn, P. L.; Serre, C.; Millange, F.; Loiseau, T.; Férey, G. *J. Am. Chem. Soc.* **2005**, *127*, 13519.
- (33) Bae, Y.-S.; Farha, O. K.; Spokoyny, A. M.; Mirkin, C. A.; Hupp, J. T.; Snurr, R. Q. *Chem. Commun.* **2008**, *4135*.
- (34) Skouidas, A. I.; Sholl, D. S. *J. Phys. Chem. B* **2005**, *109*, 15760.
- (35) Wehring, M.; Gascon, J.; Dubbeldam, D.; Kapteijn, F.; Snurr, R. Q.; Stallmach, F. *J. Phys. Chem. C* **2010**, *114*, 10527.
- (36) Haldoupis, E.; Nair, S.; Sholl, D. S. *J. Am. Chem. Soc.* **2010**, *132*, 7528.
- (37) Stallmach, F.; Gröger, S.; Künzel, V.; Kärger, J.; Yaghi, O. M.; Hesse, M.; Müller, U. *Angew. Chem., Int. Ed.* **2006**, *45*, 2123.
- (38) Zybaylo, O.; Shekhah, O.; Wang, H.; Tafipolsky, M.; Schmid, R.; Johannsmann, D.; Wall, C. *Phys. Chem. Chem. Phys.* **2010**, *12*, 8092.
- (39) Song, F.; Wang, C.; Falkowski, J. M.; Ma, L.; Lin, W. *J. Am. Chem. Soc.* **2010**, *132*, 15390.
- (40) Lee, C. Y.; Bae, Y. S.; Jeong, N. C.; Farha, O. K.; Sarjeant, A. A.; Stern, C. L.; Nickias, P.; Snurr, R. Q.; Hupp, J. T.; Nguyen, S. T. *J. Am. Chem. Soc.* **2011**, *133*, 5228.
- (41) Kortunov, P. V.; Heinke, L.; Arnold, M.; Nedellec, Y.; Jones, D. J.; Caro, J.; Kärger, J. *J. Am. Chem. Soc.* **2007**, *129*, 8041.
- (42) Chui, S. S. Y.; Lo, S. M. F.; Charmant, J. P. H.; Orpen, A. G.; Williams, I. D. *Science* **1999**, *283*, 1148.
- (43) Wang, Q. M.; Shen, D. M.; Bulow, M.; Lau, M. L.; Deng, S. G.; Fitch, F. R.; Lemcoff, N. O.; Semanscin, J. *Microporous Mesoporous Mater.* **2002**, *55*, 217.
- (44) Allendorf, M. D.; Houk, R. J. T.; Andruszkiewicz, L.; Talin, A. A.; Pikarsky, J.; Choudhury, A.; Gall, K. A.; Hesketh, P. J. *J. Am. Chem. Soc.* **2008**, *130*, 14404.
- (45) Mintova, S.; Mo, S. Y.; Bein, T. *Chem. Mater.* **2001**, *13*, 901.
- (46) Lu, G.; Hupp, J. T. *J. Am. Chem. Soc.* **2010**, *132*, 7832.
- (47) Greathouse, J. A.; Ockwig, N. W.; Criscenti, L. J.; Guilinger, T. R.; Pohl, P.; Allendorf, M. D. *Phys. Chem. Chem. Phys.* **2010**, *12*, 12621.
- (48) Feng, P. L.; Branson, J. V.; Hattar, K.; Vizkelethy, G.; Allendorf, M. D.; Doty, F. P. *Nucl. Instrum. Methods Phys. Res., Sect. A*, in press.
- (49) Lu, Z.-Z.; Zhang, R.; Li, Y.-Z.; Guo, Z.-J.; Zheng, H.-G. *J. Am. Chem. Soc.* **2011**, *133*, 4172.
- (50) Beauvais, L. G.; Shores, M. P.; Long, J. R. *J. Am. Chem. Soc.* **2000**, *122*, 2763.
- (51) Lee, H.; Jung, S. H.; Han, W. S.; Moon, J. H.; Kang, S.; Lee, J. Y.; Jung, J. H.; Shinkai, S. *Chem.-Eur. J.* **2011**, *17*, 2823.
- (52) Kreno, L. E.; Hupp, J. T.; Van Duyne, R. P. *Anal. Chem.* **2010**, *82*, 8042.
- (53) Sadakiyo, M.; Yamada, T.; Kitagawa, H. *J. Am. Chem. Soc.* **2009**, *131*, 9906.
- (54) Achmann, S.; Hagen, G.; Kita, J.; Malkowsky, I. M.; Kiener, C.; Moos, R. *Sensors* **2009**, *9*, 1574.
- (55) Biemmi, E.; Darga, A.; Stock, N.; Bein, T. *Microporous Mesoporous Mater.* **2008**, *114*, 380.
- (56) Ameloot, R.; Stappers, L.; Fransaer, J.; Alaerts, L.; Sels, B. F.; De Vos, D. E. *Chem. Mater.* **2009**, *21*, 2580.
- (57) Ohba, M.; Yoneda, K.; Kitagawa, S. *CrystEngComm* **2010**, *12*, 159.

- (58) Kepert, C. J. *J. Chem. Commun.* **2006**, 695.
- (59) Zacher, D.; Shekhah, O.; Wöll, C.; Fischer, R. A. *Chem. Soc. Rev.* **2009**, 38, 1418.
- (60) Shekhah, O.; Liu, J.; Fischer, R. A.; Wöll, C. *Chem. Soc. Rev.* **2011**, 40, 1081.
- (61) Shekhah, O.; Wang, H.; Kowarik, S.; Schreiber, F.; Paulus, M.; Tolan, M.; Sternemann, C.; Evers, F.; Zacher, D.; Fischer, R. A.; Wöll, C. *J. Am. Chem. Soc.* **2007**, 129, 15118.
- (62) Schoedel, A.; Scherb, C.; Bein, T. *Angew. Chem., Int. Ed.* **2010**, 49, 7225.
- (63) Biemmi, E.; Scherb, C.; Bein, T. *J. Am. Chem. Soc.* **2007**, 129, 8054.
- (64) Zacher, D.; Baunemann, A.; Hermes, S.; Fischer, R. A. *J. Mater. Chem.* **2007**, 17, 2785.
- (65) Scherb, C.; Schoedel, A.; Bein, T. *Angew. Chem., Int. Ed.* **2008**, 47, 5777.
- (66) Demessence, A.; Horcajada, P.; Serre, C.; Boissiere, C.; Grosso, D.; Sanchez, C.; Férey, G. *Chem. Commun.* **2009**, 7149.
- (67) Qiu, L.-G.; Li, Z.-Q.; Wu, Y.; Wang, W.; Xu, T.; Jiang, X. *Chem. Commun.* **2008**, 3642.
- (68) Zou, X.; Zhu, G.; Hewitt, I. J.; Sun, F.; Qiu, S. *Dalton Trans.* **2009**, 3009.
- (69) Qiu, Y.; Deng, H.; Mou, J.; Yang, S.; Zeller, M.; Batten, S. R.; Wu, H.; Li, J. *Chem. Commun.* **2009**, 5415.
- (70) Basabe-Desmonts, L.; Reinhoudt, D. N.; Crego-Calama, M. *Chem. Soc. Rev.* **2007**, 36, 993.
- (71) Xie, Z.; Ma, L.; deKrafft, K. E.; Jin, A.; Lin, W. *J. Am. Chem. Soc.* **2009**, 132, 922.
- (72) An, J. Y.; Shade, C. M.; Chengelis-Czegan, D. A.; Petoud, S.; Rosi, N. L. *J. Am. Chem. Soc.* **2011**, 133, 1220.
- (73) Lan, A.; Li, K.; Wu, H.; Olson, D. H.; Emge, T. J.; Ki, W.; Hong, M.; Li, J. *Angew. Chem., Int. Ed.* **2009**, 48, 2334.
- (74) Pramanik, S.; Zheng, C.; Zhang, X.; Emge, T. J.; Li, J. *J. Am. Chem. Soc.* **2011**, 133, 4153.
- (75) Bauer, C. A.; Timofeeva, T. V.; Settersten, T. B.; Patterson, B. D.; Liu, V. H.; Simmons, B. A.; Allendorf, M. D. *J. Am. Chem. Soc.* **2007**, 129, 7136.
- (76) Takashima, Y.; Martinez, V. M.; Furukawa, S.; Kondo, M.; Shimomura, S.; Uehara, H.; Nakahama, M.; Sugimoto, K.; Kitagawa, S. *Nat. Commun.* **2011**, 2, 168.
- (77) Doty, F. P.; Bauer, C. A.; Skulan, A. J.; Grant, P. G.; Allendorf, M. D. *Adv. Mater.* **2009**, 21, 95.
- (78) Willets, K. A.; Van Duyne, R. P. *Annu. Rev. Phys. Chem.* **2007**, 58, 267.
- (79) Yazaydin, A. O.; Benin, A. I.; Faheem, S. A.; Jakubczak, P.; Low, J. J.; Willis, R. R.; Snurr, R. Q. *Chem. Mater.* **2009**, 21, 1425.
- (80) Chowdhury, P.; Bikkina, C.; Meister, D.; Dreisbach, F.; Gumma, S. *Microporous Mesoporous Mater.* **2009**, 117, 406.
- (81) Herminjard, S.; Sirigu, L.; Herzog, H. P.; Studemann, E.; Crottini, A.; Pellaux, J.-P.; Gresch, T.; Fischer, M.; Faist, J. *Opt. Express* **2009**, 17, 293.
- (82) Meilikhov, M.; Yusenko, K.; Esken, D.; Turner, S.; Van Tendeloo, G.; Fischer, R. A. *Eur. J. Inorg. Chem.* **2010**, 3701.
- (83) Lu, G.; Farha, O. K.; Kreno, L. E.; Schoenecker, P. M.; Walton, K. S.; Van Duyne, R. P.; Hupp, J. T. *Adv. Mater.* **2011**, 23, 4449.
- (84) Seiyama, T.; Kato, A.; Fujiishi, K.; Nagatani, M. *Anal. Chem.* **1962**, 34, 1502.
- (85) Hu, Y.; Tan, O. K.; Cao, W.; Zhu, W. In *Sensors for Chemical and Biological Applications*; Ram, M. K., Bhethanabotla, V. R., Eds.; CRC Press: Boca Raton, FL, 2010; pp 1–42.
- (86) Grate, J. W. *Chem. Rev.* **2000**, 100, 2627.
- (87) Goeders, K. M.; Colton, J. S.; Bottomley, L. A. *Chem. Rev.* **2008**, 108, 522.
- (88) Merlijn van Spengen, W. *Microelectron. Reliab.* **2003**, 43, 1049.
- (89) Wan, Y. S. S.; Chau, J. L. H.; Gavriilidis, A.; Yeung, K. L. *Microporous Mesoporous Mater.* **2001**, 42, 157.
- (90) Mintova, S.; Bein, T. *Microporous Mesoporous Mater.* **2001**, 50, 159.
- (91) Choi, S. Y.; Lee, Y.-J.; Park, Y. S.; Ha, K.; Yoon, K. B. *J. Am. Chem. Soc.* **2000**, 122, 5201.
- (92) Sasaki, I.; Tsuchiya, H.; Nishioka, M.; Sadakata, M.; Okubo, T. *Sens. Actuators, B* **2002**, 86, 26.
- (93) Xu, X.; Wang, J.; Long, Y. *Sens. Actuators, B* **2006**, 6, 1751.
- (94) Chen, Z.; Lu, C. *Sens. Lett.* **2005**, 3, 274.
- (95) Robinson, A. L.; Allendorf, M. D.; Stavila, V.; Thornberg, S. M. *Materials Research Society Proceedings*; San Francisco, CA, April 2011.
- (96) Küsgens, P.; Rose, M.; Senkovska, I.; Froede, H.; Henschel, A.; Siegle, S.; Kaskel, S. *Microporous Mesoporous Mater.* **2009**, 120, 325.
- (97) Chakraborty, S.; Hara, K.; Lai, P. T. *Rev. Sci. Instrum.* **1999**, 70, 1565.
- (98) Lee, J. H.; Houk, R. T. J.; Robinson, A.; Greathouse, J. A.; Thornberg, S. M.; Allendorf, M. D.; Hesketh, P. J. *Proc. SPIE* **2010**, 767927.
- (99) Kitagawa, S.; Matsuda, R. *Coord. Chem. Rev.* **2007**, 251, 2490.
- (100) Fletcher, A. J.; Thomas, K. M.; Rosseinsky, M. J. *J. Solid State Chem.* **2005**, 178, 2491.
- (101) Prestipino, C.; Regli, L.; Vitillo, J. G.; Bonino, F.; Damin, A.; Lamberti, C.; Zecchina, A.; Solari, P. L.; Kongshaug, K. O.; Bordiga, S. *Chem. Mater.* **2006**, 18, 1337.
- (102) Tan, J. C.; Cheetham, A. K. *Chem. Soc. Rev.* **2011**, 40, 1059.
- (103) Munuera, C.; Shekhah, O.; Wang, H.; Wöll, C.; Ocal, C. *Phys. Chem. Chem. Phys.* **2008**, 10, 7257.
- (104) Metal-Organic Frameworks: Applications from Catalysis to Gas Storage, 1st ed.; Farrusseng, D., Ed.; Wiley-VCH: New York, 2011.
- (105) Vaidhyanathan, R.; Bradshaw, D.; Rebilly, J. N.; Barrio, J. P.; Gould, J. A.; Berry, N. G.; Rosseinsky, M. J. *Angew. Chem., Int. Ed.* **2006**, 45, 6495.
- (106) Murray, L. J.; Dinca, M.; Yano, J.; Chavan, S.; Bordiga, S.; Brown, C. M.; Long, J. R. *J. Am. Chem. Soc.* **2010**, 132, 7856.
- (107) McKinlay, A. C.; Xiao, B.; Wragg, D. S.; Wheatley, P. S.; Megson, I. L.; Morris, R. E. *J. Am. Chem. Soc.* **2008**, 130, 10440.
- (108) Doleman, B. J.; Lonergan, M. C.; Severin, E. J.; Vaid, T. P.; Lewis, N. S. *Anal. Chem.* **1998**, 70, 4177.
- (109) Dickinson, T. A.; White, J.; Kauer, J. S.; Walt, D. R. *Nature* **1996**, 382, 697.
- (110) Rakow, N. A.; Suslick, K. S. *Nature* **2000**, 406, 710.
- (111) Wilmer, C. E.; Leaf, M.; Lee, C. Y.; Farha, O. K.; Hauser, B. G.; Hupp, J. T.; Snurr, R. Q. *Nat. Chem.*, in press, DOI: 10.1038/NCHEM.1192.
- (112) FitzGerald, S. A.; Allen, K.; Landerman, P.; Hopkins, J.; Matters, J.; Myers, R.; Rowsell, J. L. *C. Phys. Rev. B* **2008**, 77, 224301.
- (113) Sugikawa, K.; Furukawa, Y.; Sada, K. *Chem. Mater.* **2011**, 23, 3132.
- (114) Vitillo, J. G.; Regli, L.; Chavan, S.; Ricchiardi, G.; Spoto, G.; Dietzel, P. D. C.; Bordiga, S.; Zecchina, A. *J. Am. Chem. Soc.* **2008**, 130, 8386.